ASSESMENT OF PATIENT RESPONSE TO TARGETED CANCER THERAPY USING MULTI-FREQUENCY IMPEDANCE CYTOMETRY AND SUPERVISED MACHINE LEARNING

by KARAN SHASHI AHUJA

A Thesis submitted to the

School of Graduate Studies

Rutgers, the State University of New Jersey

in partial fulfillment of the requirements

for the degree of

Master of Science

Graduate Program in Electrical and Computer Engineering

Written under the direction of

Dr. Mehdi Javanmard

and approved by

_____

_____

_____

_____

New Brunswick, New Jersey

May 2018

ABSTRACT OF THE THESIS

ASSESMENT OF PATIENT RESPONSE TO TARGETED CANCER THERAPY USING MULTI-FREQUENCY IMPEDANCE CYTOMETRY AND SUPERVISED MACHINE LEARNING

by KARAN SHASHI AHUJA

THESIS DIRECTOR:

Dr. Mehdi Javanmard

We present a novel method to rapidly assess patient response to targeted cancer therapy, where anti-neoplastic agents are conjugated to antibodies targeting surface markers on tumor cells. We have fabricated and characterized a device capable of rapidly assessing tumor cell viability in response to the drug using multi-frequency impedance spectroscopy in combination with supervised machine learning for enhanced classification accuracy. Currently commercially available devices for the analysis of cell viability are based on staining with Trypan blue. Staining fundamentally limits the subsequent characterization of these cells as well as further molecular analysis, and requires 0.5-1.0 milliliter of

volume. Our approach only requires 50 microliters of volume and avoids staining allowing for further molecular analysis. To the best of our knowledge, this work presents the first comprehensive attempt in using phase change obtained from impedance cytometry data to assess viability of cells. Use of impedance cytometry to quantify cancer cells from blood cells was also explored.

ACKNOWLEGMENTS

First and foremost, I would like to thank Dr. Mehdi Javanmard for giving me the opportunity to be a part of Nano Bio Electronics laboratory. Without his valuable guidance and direction, I would not have been able to complete my Master's Thesis. I was a part of several projects under him which helped me to gain significant knowledge in the field of biosensors and bioelectronics.

I am grateful to PhRMA foundation for funding this work. I would like to specially thank my collaborators from Rutgers Cancer Institute of New Jersey, Dr. J. R. Bertino and Dr. G. M. Rather for providing valuable insights and samples for this project. I am also grateful to all members of Microelectronics Research Laboratory (MERL) at Rutgers University for assisting me in the fabrication processes. Without their valuable help and time, I would not have been able to fabricate sensors and microfluidic channels for my project.

I am thankful to Dr. Zoran Gajic, Dr. Laura Fabris and Dr. Michael Wu for being a part of my Master's Thesis committee. The feedback provided by them on my work would be very valuable and helpful to me.

I wish to specially thank all the members of my lab: Jianye Sui, Tuan Le, Pengfei Xie, Azam Gholizadeh, Kavya Vasudevamurthy, Zhongtian Lin, Sakshi Sardar and Abbas Furniterwala for constantly supporting me in my projects. All the ideas and discussions with them helped me to leverage my knowledge and I got to learn many new things from all the lab members.

I would also like to thank Tea Akkins, John Scafidi, Arletta Hoscilowicz, Steve Orbine and Robert Lorber for their help and assistance in my projects. I also extend my gratitude towards Shawn Taylor (School of Management and Labor Studies, Rutgers University) for helping me while writing my thesis.

Last, but not the least I would like to thank my parents for their consistent support and trust, my friends who always motivated me in tough times and all the faculty which served as a constant motivation for me to excel.

TABLE OF CONTENTS

ABSTRACT……. ii

ACKNOWLEDGMENTS…….. iv

LIST OF TABLES…….. vi

LIST OF FIGURES……..... ix

1. Introduction

1.1 Cancer and Targeted Cancer Therapy……. 1

1.2 Research Goals…… 3

1.3 Thesis Organization……. 4

2. Cell Viability Analysis

2.1 Trypan Blue Dye Exclusion Method……... 6

2.2 Optical Coherence Tomography…….. 8

2.3 Microfluidic Platforms to Analyze Cell Viability……... 8

3. Methodology

3.1 Proposed Approach…….. 10

3.2 Device Fabrication

3.2.1 Sensor Fabrication…….. 11

3.2.2 Fabrication of Master Mold……..... 13

3.2.3 Soft Lithography…… 15

3.2.4 Device Bonding…….. 17

3.3 Electrical Impedance Cytometry……. 18

3.4 Cell Culture…….. 19

3.5 Signal Processing and Machine Learning……... 22

4. Results and Discussions

4.1 Support Vector Machine Classifier……. 24

4.2 Performance of SVM Classifier…….. 26

4.3 Amplitude Change as Feature for Classification……. 26

4.4 Phase Change as Feature for Classification……. 32

4.5 Amplitude Change and Phase Change as Feature for Classification……. 35

5. Exploring use of Impedance Cytometry for Quantification of Cancer Cells in Blood Cells……. 38

6. Conclusion and Future Scope…… 42

7. Appendix

7.1 Oxygen Plasma Etching……... 43

7.2 Support Vector Machine…….. 43

8. Bibliography…… 45

LIST OF TABLES

Table 5.1 Accuracy of different machine learning classifiers to classify between cancer cells and blood cells..... 42

LIST OF FIGURES

Figure 1.1 Illustration of normal cells dividing…….. 1

Figure 1.2 Illustration of abnormal cells dividing…… 2

Figure 1.3 Targeted Cancer Therapy…….. 4

Figure 2.1 Trypan blue dye exclusion method……... 6

Figure 2.2 Vi-Cell Analyzer……... 7

Figure 2.3 Fluorescence imaging for analysis of cell viability …….. 9

Figure 3.1 Schematic diagram of the system…….. 10

Figure 3.2 Processes involved in sensor fabrication……... 12

Figure 3.3 Picture of fabricated sensors……. 13

Figure 3.4 Process involved in fabrication of master mold…… 14

Figure 3.5 Picture of fabricated master mold……. 15

Figure 3.6 Soft lithography …… 16

Figure 3.7 Picture of PDMS microfluidic channel bonded to electrodes……..... 17

Figure 3.8 Microfabricated electrodes at the channel……. 18

Figure 3.9 Simplified schematic of an impedance cytometer…… 20

Figure 3.10 Equivalent circuit model …… 21

Figure 4.1 Normalized impedance response of live cancer cells……... 27

Figure 4.2 Normalized impedance response of dead cancer cells…….. 27

Figure 4.3 Amplitude spectrum of live and dead cancer cells…… 28

Figure 4.4 Scatter plot of live and dead cancer cells at 500KHz and 20MHz ……... 29

Figure 4.5 Scatter plot of live and dead cancer cells at 500KHz and 25MHz……..... 29

Figure 4.6 Scatter plot of live and dead cancer cells at 500KHz and 30MHz…… 30

Figure 4.7 Confusion matrix of the SVM classifier while using impedance change as feature…….. 31

Figure 4.8 Comparison between analysis of cell viability by using trypan blue staining and multi-frequency impedance cytometry with SVM……..... 31

Figure 4.9 Scatter plot of phase change for live and dead cancer cells at 500KHz and 20MHz……..... 32

Figure 4.10 Scatter plot of phase change for live and dead cancer cells at 500KHz and 25MHz……... 33

Figure 4.11 Scatter plot of phase change for live and dead cancer cells at 500KHz and 30MHz……... 33

Figure 4.12 Confusion matrix of the SVM classifier while using phase change as feature…… 34

Figure 4.13 Comparison between analysis of cell viability by using trypan blue staining and multi-frequency impedance cytometry with SVM…… 35

Figure 4.14 Confusion matrix of the SVM classifier while using phase change and amplitude change as feature…… 36

Figure 4.15 Comparison between analysis of cell viability by using trypan blue staining and multi-frequency impedance cytometry with SVM…… 37

Figure 5.1 Schematic diagram of the system to explore quantification of cancer cells in blood……... 39

Figure 5.2 Scatter plots of live cancer cells and blood cells at 1500KHz and 1MHz……... 40

Figure 5.3 Scatter plots of live cancer cells and blood cells at 500KHz and 20MHz……. 40

Figure 5.4 Normalized amplitude response of live cancer cells……. 41

Figure 5.5 Normalized amplitude response of blood cells……. 41

Chapter 1

Introduction

1.1 Cancer and Targeted Therapy

Cancer is one of the diseases which continuously threatens human life. It accounts to 13% of the deaths worldwide [1]. It is a disease in which abnormal cells divide uncontrollably and destroy body tissues. Cancer can occur anywhere in the human body. Normally, human cells grow and divide to form new cells as the body needs them. When normal human cells grow old or become damaged, they die, and new cells take their place. When cancer develops, however, this orderly process breaks down. As cells become abnormal, old or damaged cells survive when they should die. Thus, new cells are formed even if they are not needed. These extra cells can divide without stopping and may form tumors [2]. Figure 1.1 and 1.2 illustrate how normal cells divide and how abnormal cells multiply uncontrollably.

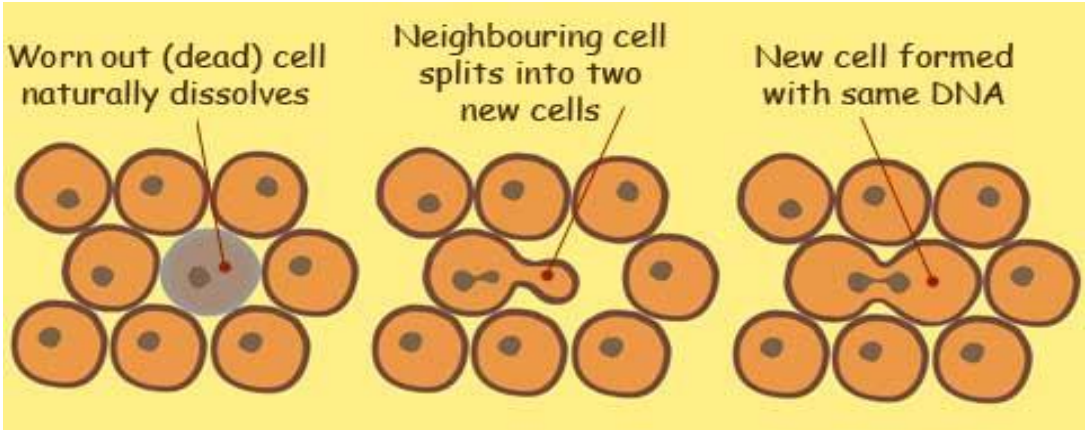

Figure 1.1. Illustration of normal cells dividing

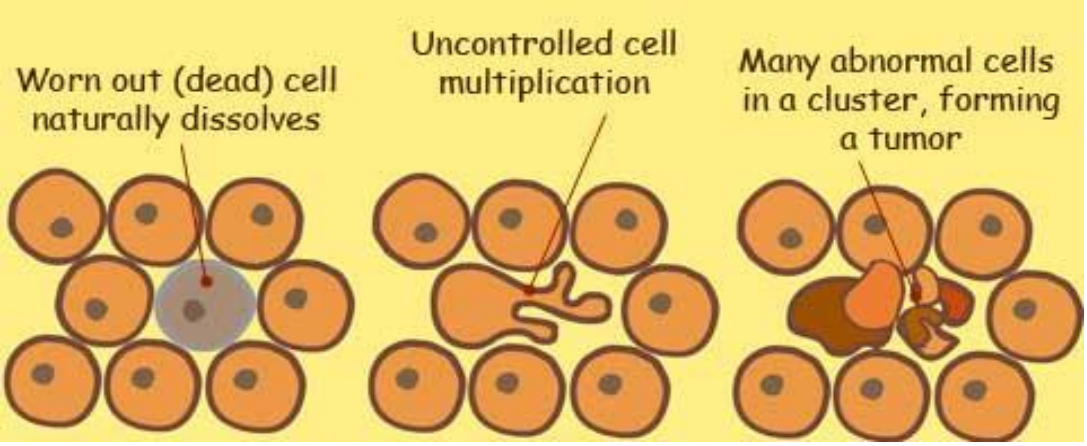

Figure 1. 2. Illustration of abnormal cells dividing, leading to tumor formation

The primary treatment options for cancer include surgery [3], chemotherapy [4], radiation therapy [5], hormonal therapy [6], targeted therapy [7] and palliative care [8]. The choice of therapy mainly depends upon type and stage of cancer, legal issues, clinical infrastructure, past response rates and patient's health conditions. Of these treatment options, a corner stone of precision medicine which uses a person's genes and proteins to prevent, diagnose and treat a disease is targeted cancer therapy [9]. Targeted therapy is a cancer treatment that uses drugs. It is different from traditional chemotherapy. The drugs known as targeted therapy help stop cancer from growing and spreading. They work by targeting specific genes or proteins. These genes and proteins are found in cancer cells or in cells related to cancer growth, like blood vessel cells [10]. In the past use of targeted cancer therapy combined with other therapies like surgery, radiation therapy etc. has proven to be useful in the treatment of cancer. In targeted cancer therapy it is very important to determine whether a patient's tumor has a specific gene mutation that codes for the target. This can be determined by analyzing the viability of tumor cells. If the tumor cells

die, the patient's tumor has a specific gene mutation coding to the target. Figure 1.3 presents a simplified version of targeted cancer therapy. Matriptase a protease which is expressed on the surface of various circulating tumor cells. Anti-matriptase antibody is conjugated with anti-neoplastic agents which are highly toxic in nature. When the anti-matriptase antibody binds to the protein, the anti-neoplastic agents specifically kill the cancer cells and do not harm blood cells.

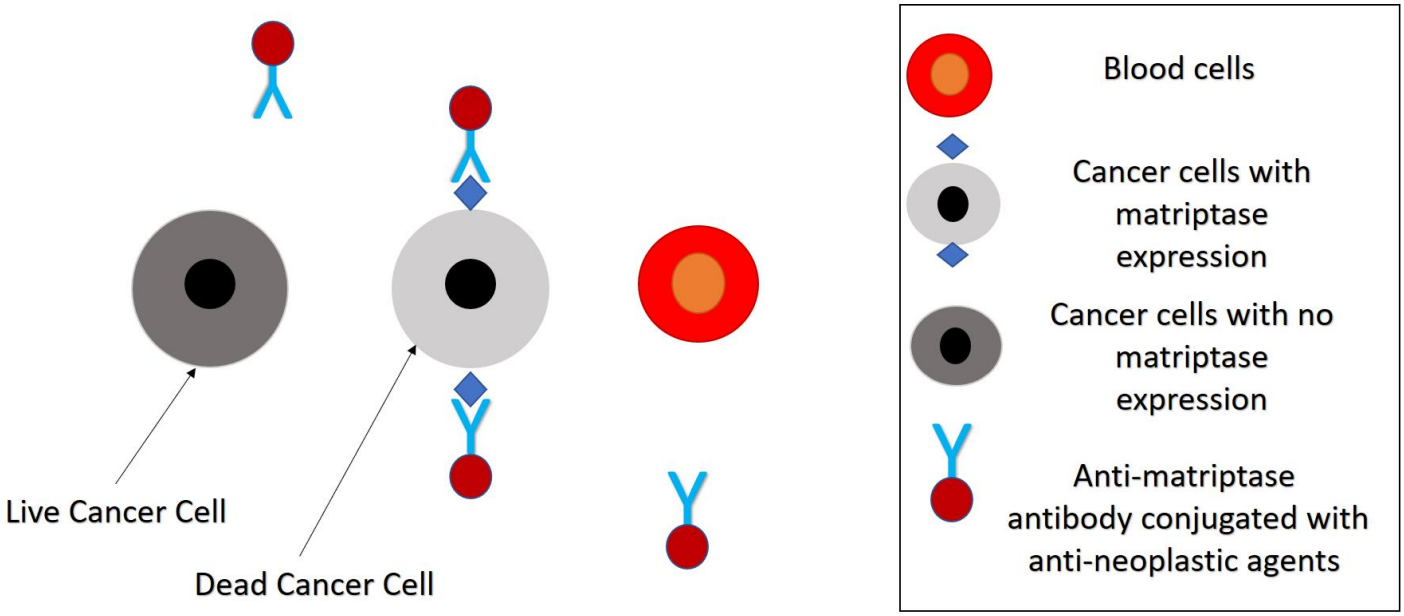

Figure 1.3. Targeted Cancer Therapy

1.2 Research Goals

In the past there has been significant development in label free separation of tumor cells from whole blood. Label free methods such as filtration, hydrodynamic chromatography and di-electrophoresis are well understood [11]. Despite significant achievement in label free separation of tumor cells, label free viability analysis of tumor cells hasn't achieved significant progress. The current techniques to analyze cell viability rely on staining.

Staining fundamentally limits the subsequent characterization of these cells as well as further molecular analysis, and requires 0.5-1 milliliter of volume.

There arises a need to develop a low cost, label free and portable device which can be used to analyze cell viability. Emerging BioMEMS technologies are showing promise to play an ever-increasing role in diagnosing chronic diseases such as cancer and infectious diseases like HIV, and proteomic and genomic studies [12,13,14]. In this work our goal was to fabricate and characterize a device capable of rapidly assessing tumor cell viability in response to the drug by using multi-frequency impedance cytometry and machine learning for enhanced classification accuracy. The use of impedance cytometry allows measurement of single-cell electrical properties. Machine learning can then be used to accurately analyze the electrical properties of tumor cells.

Microfluidic impedance based cytometry has advantages of being label-free, compatible with mass manufacturing, inexpensive, requirement of low sample volume, and it can be miniaturized into a small instrument with tiny foot print. In this work we also extended the analysis of impedance cytometry data. We have worked on metrics such as impedance change and phase change at various frequencies to assess cell viability.

1.3 Thesis Organization

Chapter 2 presents an overview of current techniques to analyze cell viability. We briefly discuss about trypan blue dye exclusion method, optical coherence chromatography (OCT) and overview of various microfluidic platforms which are used to analyze cell viability. We also look at commercially available product to analyze cell viability and discuss advantages of each technique.

Chapter 3 focuses on our novel approach to analyze cell viability. We first discuss in brief about impedance cytometry in chapter 3.1. In chapter 3.2 we look at the steps involved in fabrication and integration of our bio-sensing device. Chapter 3.3 focuses on the sample preparations and anti-matriptase drug. Chapter 3.4 introduces about machine learning and its applications, especially in the BioMEMS field.

In chapter 4 we have a look at results and discuss more about our approach. We discuss about the electrical model of a cell proposed in literature. We also look at how Support Vector Machine (SVM) is used to classify cells. We analyze the results in detail and make a comprehensive attempt to use phase change as an important feature for classification. We compare our approach with the current gold standard i.e Trypan Blue Dye Exclusion method.

In chapter 5 we discuss how we used this novel platform technology to quantify cancer cells in blood cells. We classified cultured cancer cells and blood cells using impedance cytometry data.

Finally, in chapter 6 we discuss about the conclusions and future scope. We discuss how we can use this novel approach can be improvised and used towards personalized therapeutics. We present how impedance cytometry is made portable which can help to develop this method as a point of care diagnostic device to assess cell viability.

Chapter 2

Cell Viability Analysis

2.1 Trypan Blue Dye Exclusion Method

Trypan blue is commonly used in microscopy (for cell counting) and in laboratory mice for assessment of tissue viability. In the field of biosciences, it is used as a vital stain to selectively color dead tissues or cells blue [15]. Trypan blue dye exclusion method is based on the principle that live cells possess intact cell membranes that exclude certain dyes, such as trypan blue or eosin whereas dead cells do not. The dye exclusion process is pictorially shown in figure 2.1.

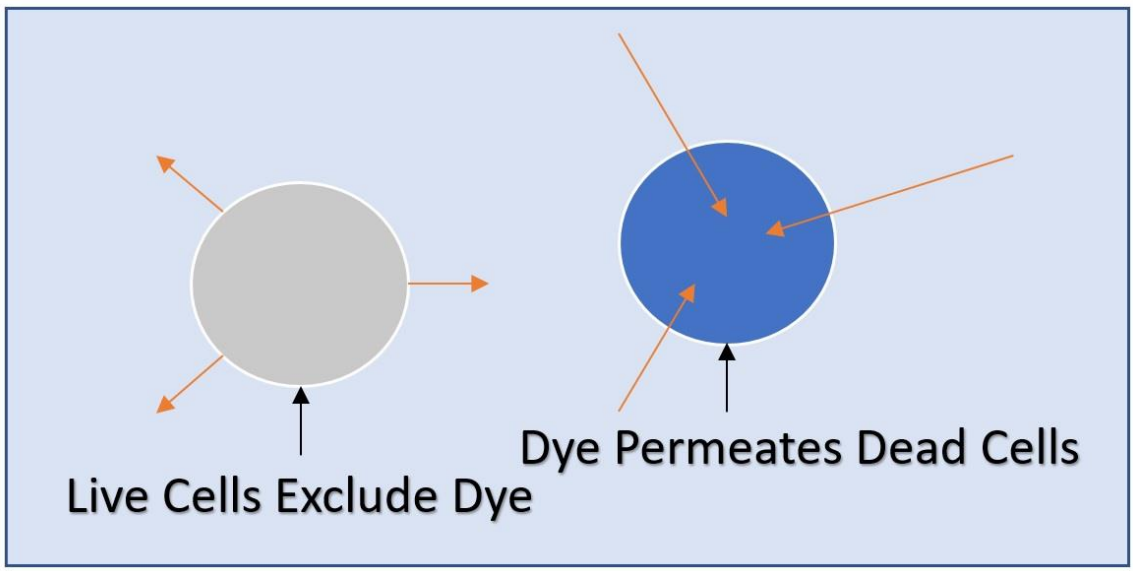

Figure 2. 1 Trypan blue dye exclusion method

The unstained (viable) and stained (dead) cells are counted under a hemocytometer and the percentage viability is calculated. The manual process of cell counting can sometime lead to inaccurate or inconsistent results. One of the commercially available product to automatically perform the trypan blue dye exclusion method is Vi-Cell Analyzer by Beckman Coulter®. This eliminates variability and thus ensures accurate results. Fig 2.2 shows an image of the Vi-Cell Analyzer.

Figur.2. Vi-Cell Analyzer used for automated viability analysis by Beckman Coulter®

Although trypan blue dye exclusion method can be used to rapidly analyze cell viability, it relies on staining which fundamentally limits subsequent characterization of cells and requires large sample volume (0.5 ml – 1ml). In addition the cost of analysis of cell viability using automated products is exorbitant.

2.2 Optical Coherence Tomography (OCT)

Optical coherence tomography (OCT) is an imaging technique that utilizes coherent light to capture micrometer-resolution, two- and three-dimensional images from within optical scattering media (e.g., biological tissue). It is widely used in medical imaging and destructive testing (NDT) [16]. Low-coherence interferometry is used in OCT to produce images of optical scattering from internal tissue microstructures [17]. A simple OCT architecture consists of a light source with a large bandwidth, a beam splitter, mirror and a spectrometer. Light from the light source is split into a sample field and reference field, the sample field is incident on the sample (target) and reference field is reflected off form a reference mirror. The recombined light is then detected using a spectrometer which then performs imaging. Recently, OCT has been used for quantitative tracking of cell death and viability in a 3D tumor model [18]. Although OCT is a label free technique to analyze cell and tissue viability, developing a point of care miniaturized system using OCT is challenging and costly.

2.3 Microfluidic platforms to analyze cell viability

To overcome the sample input problem, microfluidic platforms have been vastly explored to analyze cell viability, dose response screening and cell culture. Various microfluidic techniques have used trypan blue staining to assess cell viability. Komen et al. demonstrated two microfluidic devices to validate cell culture and analyze chemo sensitivity of MCF-7 cells [38]. Again, some form of staining was used to assess the viability of cells, Calcein-AM (CAAM; Molecular Probes Invitrogen) and 10 μg/ml Propidium Iodide (PI; Sigma, St. Louis, MO, USA) was used.

Swastika et al. demonstrated a microfluidic platform to analyze viability in tumor clusters and single cells. Here the live dead cell imaging kit by Life Technologies was used to perform the assay [39].

Mazutis et. al explored droplet microfluidics to analyze and sort singe cells [40]. The Schematic of their system is shown in figure 2.3. Fluorescence techniques were used to analyze antigen-antibody interaction. Fluorescent die was thus used to analyze cell viability.

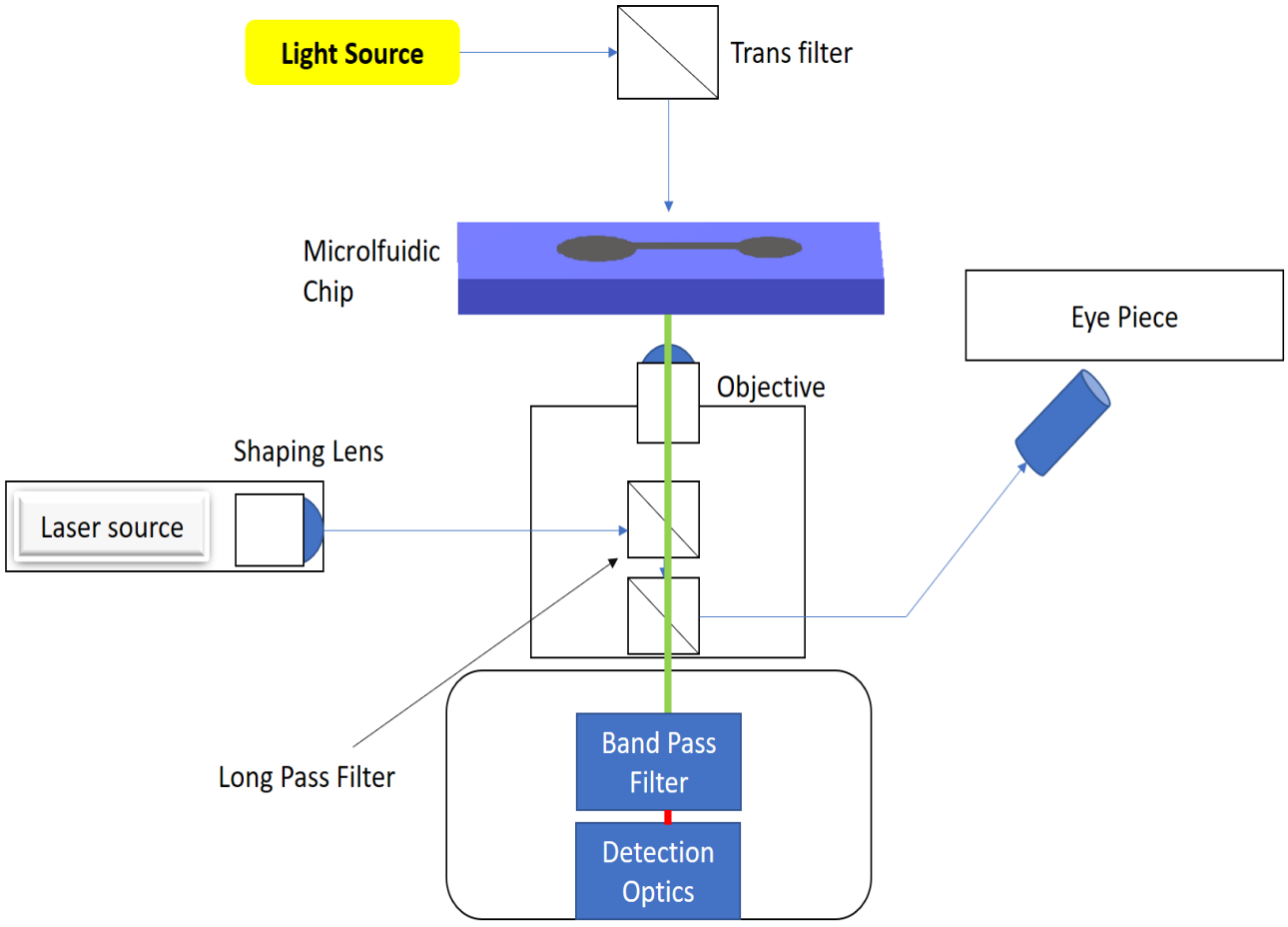

Figure 2.3 Fluorescence imaging utilized by Mazutis et. al to analyze cell viability.

Chapter 3

Methodology

3.1 Proposed Approach

Figure 3.1 presents the block diagram of our system. It consists of microfluidic channel embedded on a glass wafer with gold electrodes, multi-frequency lock-in amplifier (Zurich Instruments®) and software to record and analyze the data. This novel approach requires only 50ul of sample and avoids staining, allowing further molecular analysis. Each individual block is explained in the following sections.

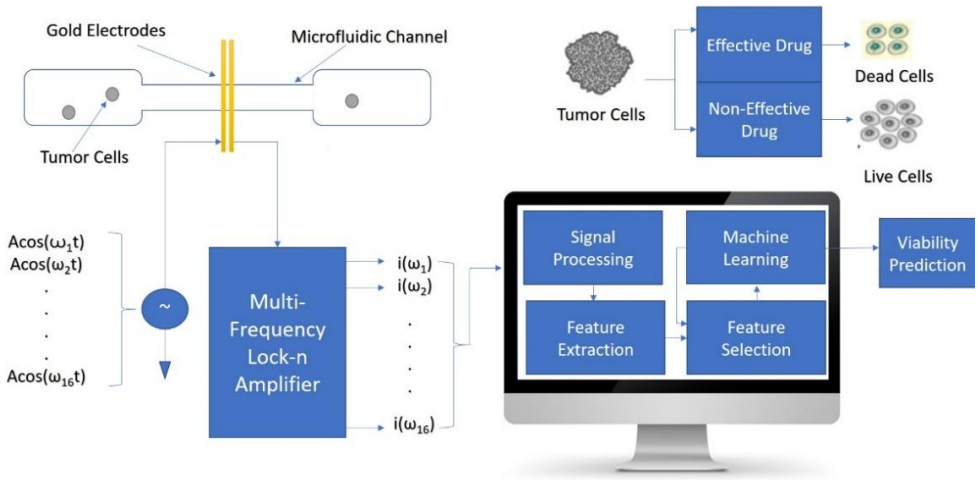

Figure 3.1. Schematic Diagram of the system. Multi-frequency impedance cytometry measures the response across a broad range of frequencies for assessment of cellular response to target drug. Live Cells and Dead Cells are assessed using machine learning algorithm to predict their viability.

3.2 Device Fabrication

Device fabrication for impedance cytometry consists of four major steps, namely: fabrication of sensor, fabrication of master mold for microfluidic channels, soft-lithography and bonding.

3.2.1 Sensor Fabrication

The fabrication process of electrodes consists of standard photolithography on a 3” fused silica wafer. The process consists of photo-patterning resist on the fused silica wafer, electron beam metal evaporation and liftoff processing. The process of photo-patterning includes wafer cleaning, spin coating the photoresist (AZ5214), soft bake of the resist, ultraviolet light exposure through a chromium mask printed on a 4” x 4” glass plate, resist development (AZ5214 MIF Developer) and hard bake of the resist. Following the photo-patterning process a 100nm gold layer is deposited on the substrate using electron beam evaporation. A 10nm layer of chromium is used to enhance the adhesion of gold film to the glass wafer; otherwise the gold film gets peeled off easily. We chose gold as the electrode due to its resistance to corrosion and inert nature. Figure 3.2 represents the processes involved in sensor fabrication and Figure 3.3 presents the fabricated sensor using these processes.

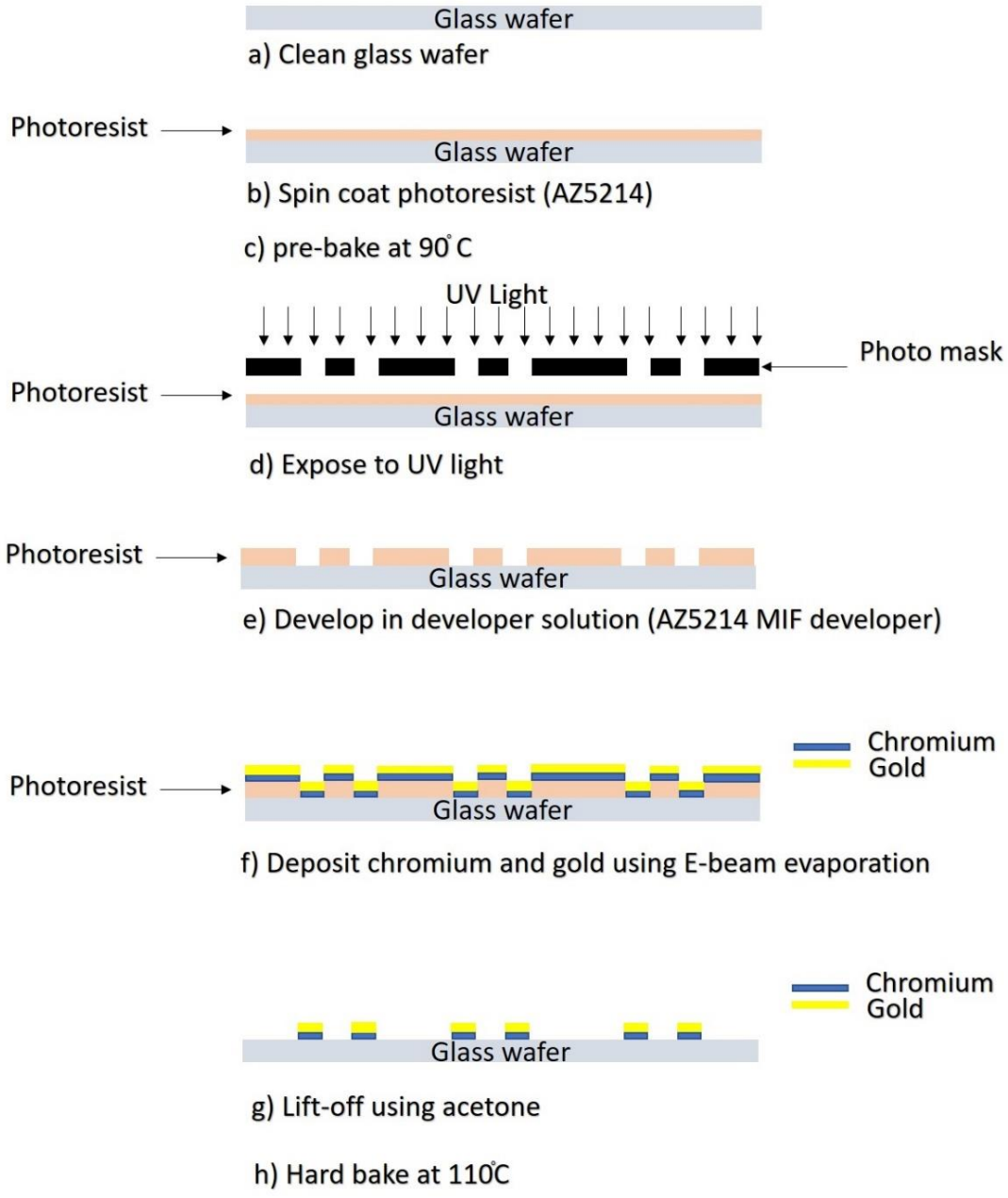

Figure 3.2. Processes involved in sensor fabrication.

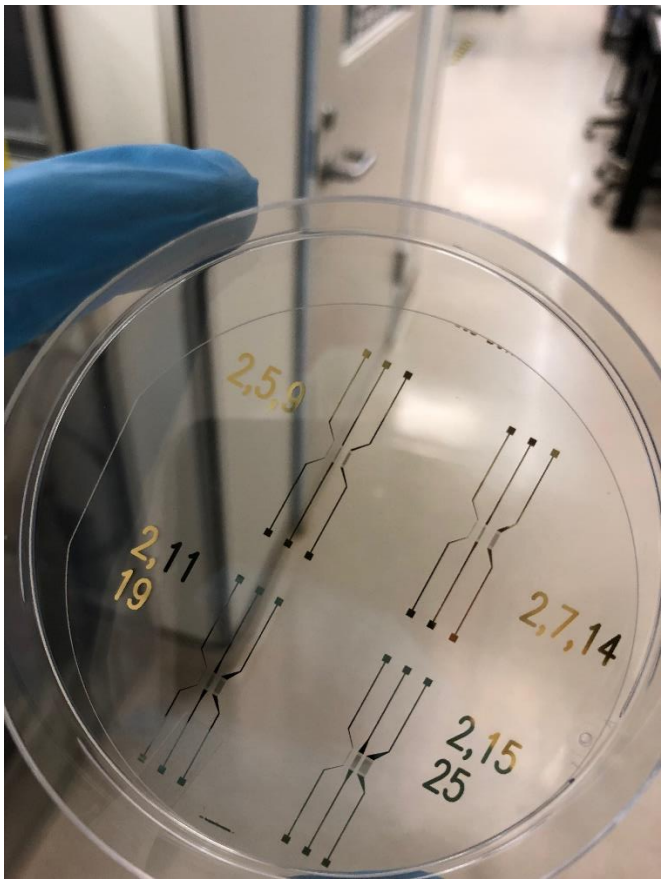

Figure 3.3. Picture of fabricated electrodes. Device also contains multi-electrodes but only 2 electrode system is used.

3.2.2 Fabrication of Master Mold for Microfluidic Channels

Fabrication of master mold for microfluidic channel consists of patterning photoresist (SU8-10) on a silicon wafer. The process of photo-patterning includes wafer cleaning, exposing the wafer to oxygen plasma, spin coating the photoresist, soft bake of the resist, ultraviolet light exposure through a chromium mask printed on a 4” x 4” glass plate, resist development (SU8-10 Developer) and hard bake of the resist. The Microfluidic channel was 100um wide and 28um high. Figure 3.4 represents the fabrication processes involved

in fabrication of master mold and Figure 3.5 presents the fabricated mold using these processes. SU8-10 is a negative photoresist, meaning the unexposed region dissolves after development. SU8-10 is highly viscous, hence the silicon wafer should be exposed to oxygen plasma prior to spin-coating which will ensure that the photoresist is spread evenly.

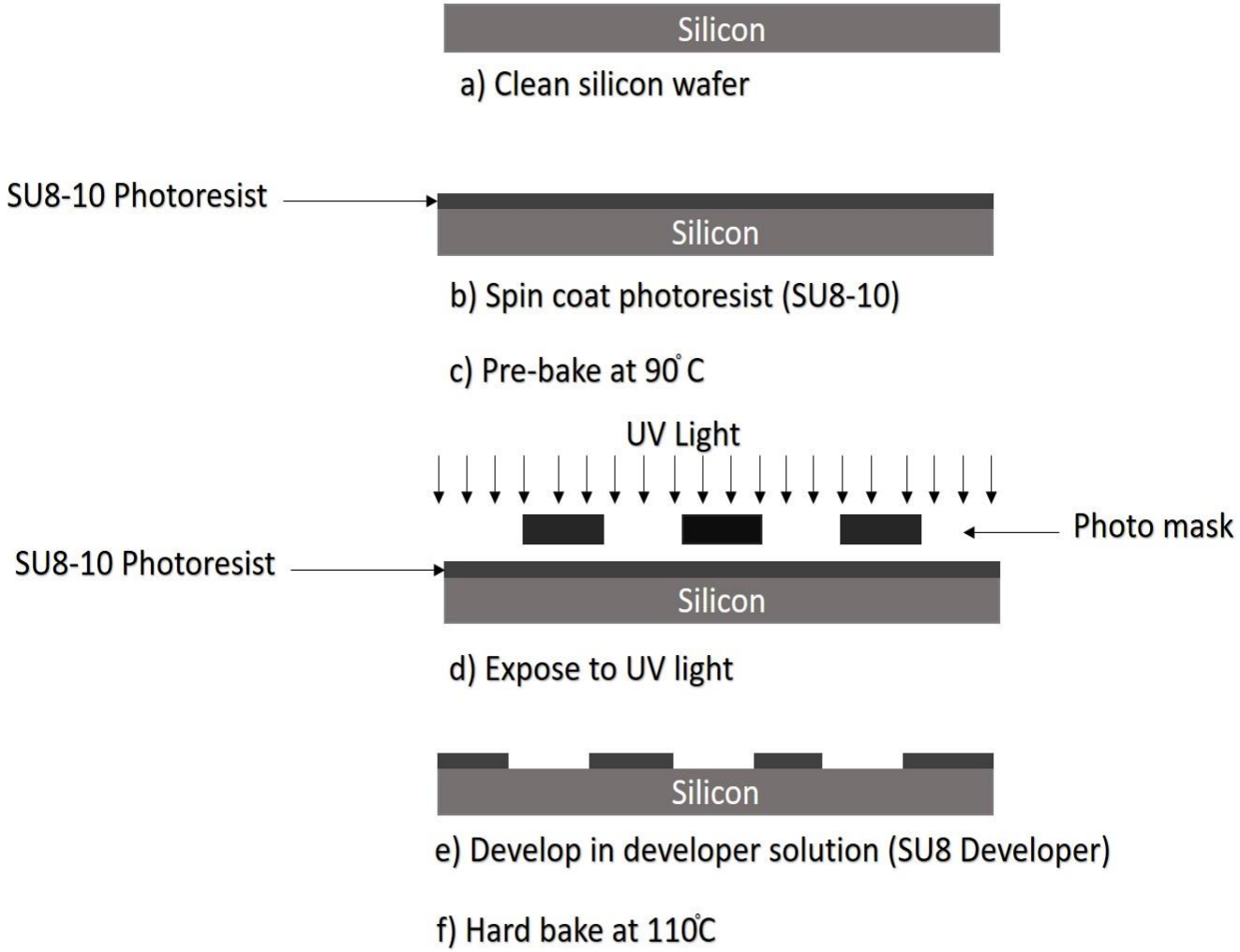

Figure 3.4 Processes involved in fabrication of master mold.

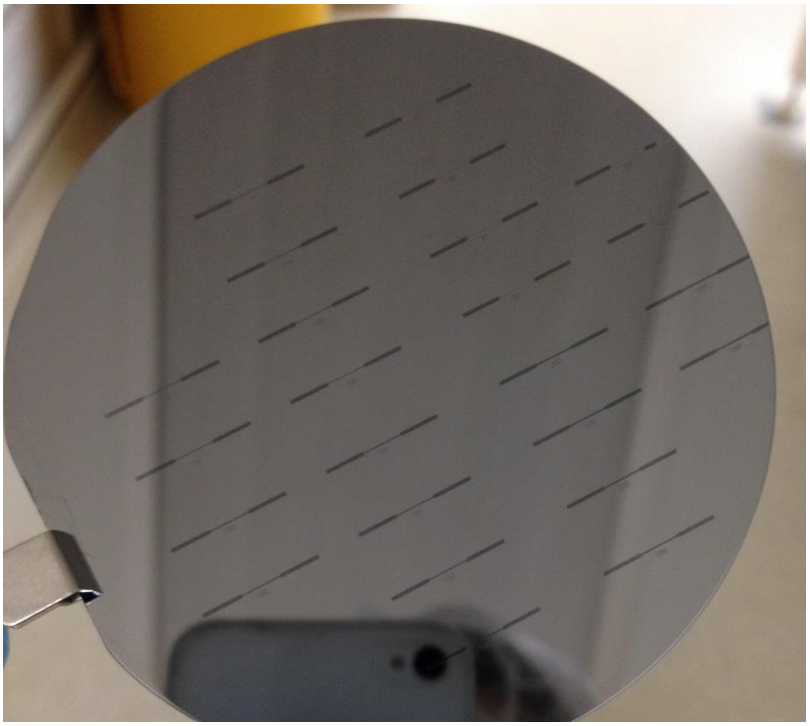

Figure 3.5. Picture of fabricated master mold. Several microfluidic channels can be then fabricated by using this mold.

3.2.3 Soft-lithography

Compared to traditional lithographic techniques, soft-lithography is well suited for applications in biotechnology and has lower cost. We used Polydimethylsiloxane (PDMS) to form microfluidic channels. PDMS is a moldable elastomer and is deformable, chemically unreactive and transparent and is thus widely used to make microfluidic channels. After the master mold was fabricated, PDMS (10:1 pre-polymer/ curing agent) was poured onto the master mold and baked at 80° C over two hours for curing. The liquid (PDMS and curing agent) is thus cured into a rubbery solid that matches the original

pattern. The PDMS channel was then peeled off from the mold. Figure 3.6 presents the processes involved in soft-lithography.

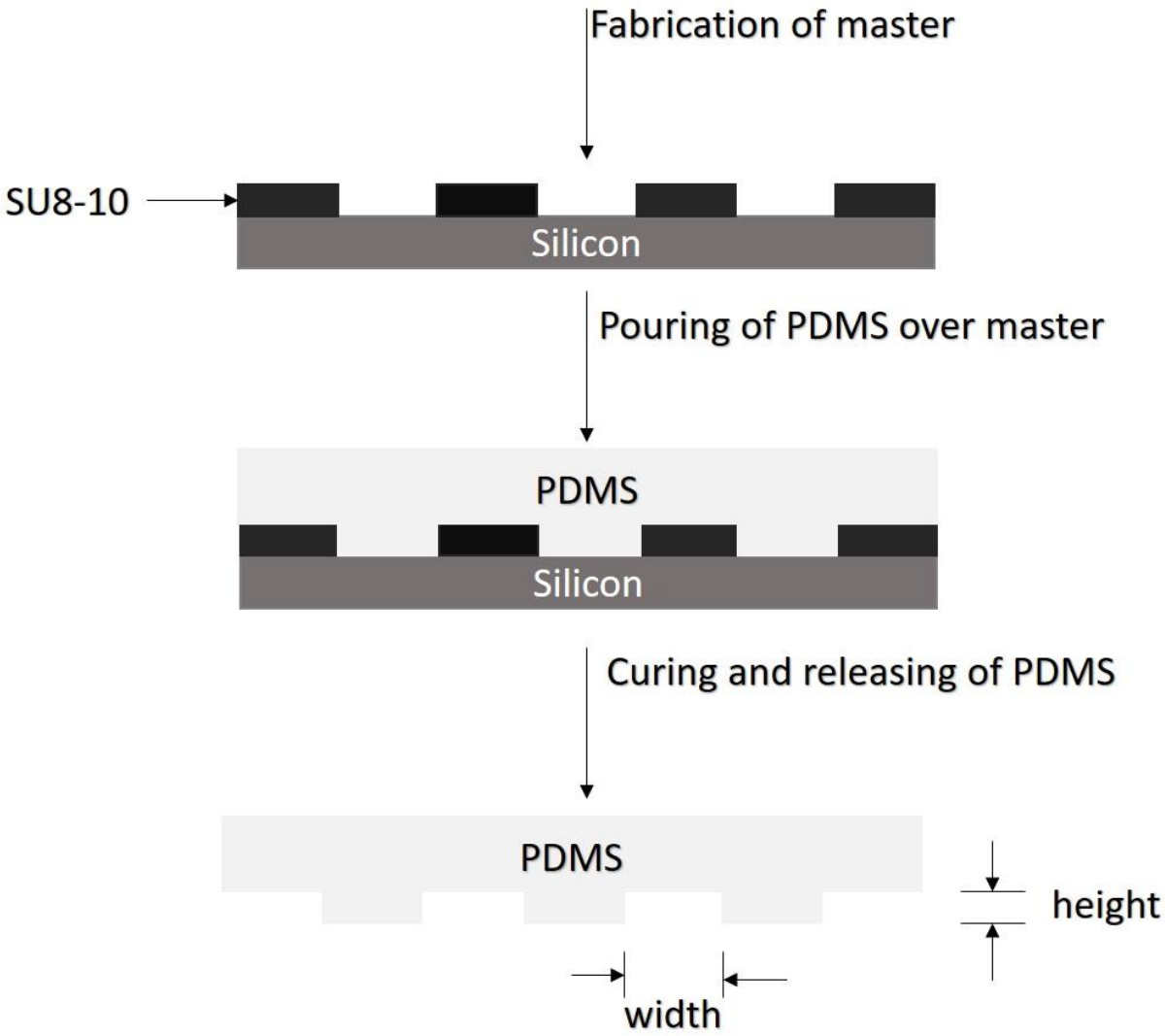

Figure 3.6. Utilizing soft-lithography to form microfluidic channels.

3.2.4 Device Bonding

Resistor lags were bonded to the sensors using epoxy and curing agent. The bonded epoxy was kept overnight to form irreversible bond. 5mm and 1.5mm holes were punched onto the cured PDMS to form inlet and outlet respectively. PDMS substrate was then cleaned with iso-propyl alcohol and sensors was cleaned using acetone. PDMS substrate was then aligned and bonded to the electrode chip after both substrates have undergone oxygen plasma treatment. The bonded chip was then baked at 70℃ for 30 minutes to form irreversible bond. Figure 3.7 represents the bonded device and Figure 3.8 presents microscopic view of microfabricated electrodes bonded with the channel.

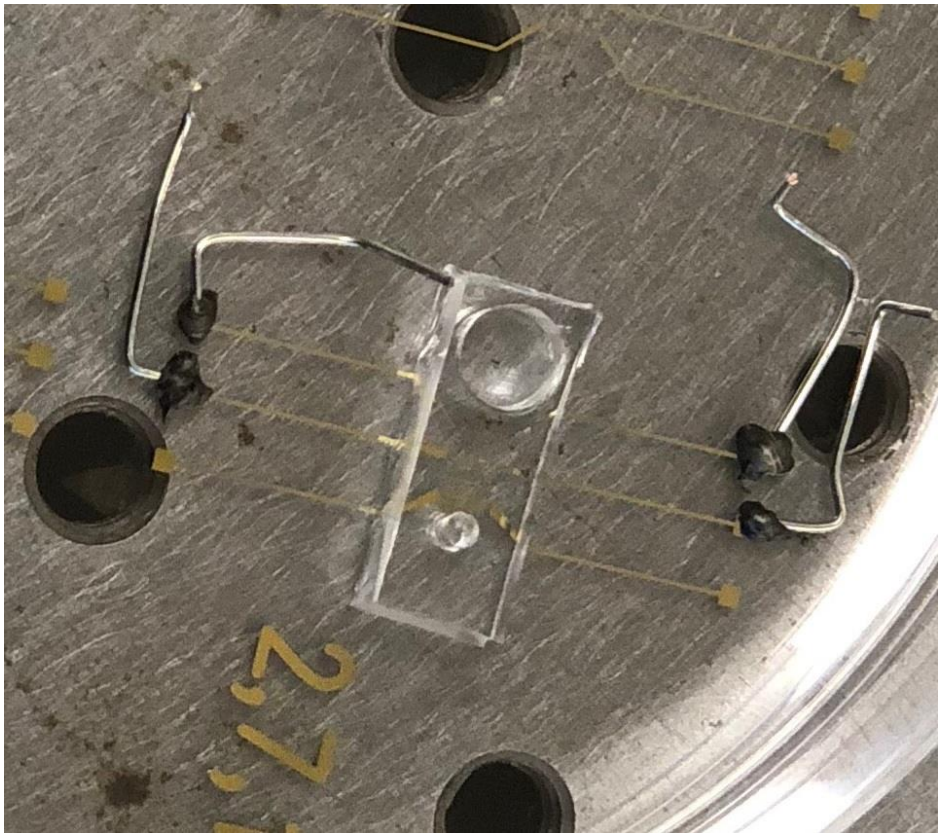

Figure 3.7. Image of PDMS microfluidic channel bonded to electrodes. The two ends of the electrodes are further connected to a multi-frequency lock-in amplifier.

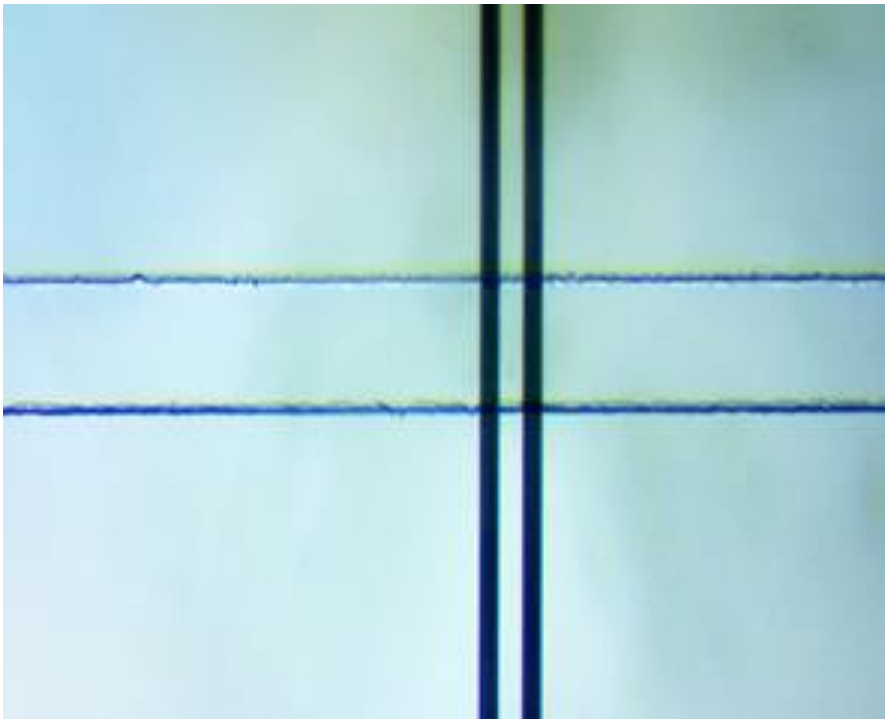

Figure 3.8. Microfabricated electrodes at the channel.

3.3 Cell Culture

For cell culture RPMI 1640 media, Dulbecco's modified Eagles medium (DMEM) and Fetal bovine serum albumin from Invitrogen (Fischer Scientific) were used. T47D cells (breast cancer cells) were cultured in RPMI 1640 media containing 10% fetal bovine serum. To perform the cytotoxicity assay seven thousand cells per well were plated in RPMI 1640/DMEM media (Gibco) supplemented with 10% FBS (Invitrogen). After overnight culture, spent media was removed and fresh media containing drug was added and plates were incubated for different time periods. To assess cell viability of breast cancer cell line (T47d cell line), at the end of the experiment 3-(4,5- dimethylthiazol-2-yl)-5- (3-carboxymethoxyphenyl)- 2-(4-sulfophenyl)-2H- tetrazolium, inner salt (MTS) assay was

performed according to the Cell Titer 96 Aqueous One Solution protocol (Promega, Madison, WI). The cytotoxicity data were further analyzed using GraphPad Prism 4 software (GraphPad Software Inc., CA). The 50% inhibitory concentration (IC50; the drug concentration required to obtain 50% cell kill compared to control) was determined using the non-linear regression curve fit of the graphs drawn by GraphPad Prism 4 software. All experiments were performed in triplicate wells and all experiments were repeated at least three times.

A subset of the cells was treated with monomethyl auristatin in conjunction with anti-matriptase antibody for targeted drug delivery. Matriptase is a protease expressed on the surface of various tumor cells. After the cell culture was performed, the cells in the media (RPMI 1640) were centrifuged (290 G for 5 minutes) and suspended in PBS to perform the impedance cytometry experiments.

3.4 Electrical Impedance Cytometry

Electrical impedance spectroscopy/ cytometry enable measuring of AC electrical properties of particles in suspension through which dielectric parameters of the particles can be obtained. The primary advantage of impedance cytometry is that it is label free and analysis can be done at a single cell level. The use of bio-impedance measurements can be dated back to the early 1910s [19-21] where low and high frequency conductivity of erythrocytes was measured. Since then there have been numerous advancements in the field of microfluidic single cell impedance analysis [22]. Microfluidic impedance cytometry has shown promising results in various fields such as analysis and differentiation

of leukocytes [23] and platelets [24], whole blood cell differentiation [25], Nano-electronic barcoding of particles [26], tumor cell characterization and classification [27] and PicoMolar level detection of protein biomarkers [28]. We extend the advancements made in impedance cytometry towards a new direction where analysis of cell viability of the cancer cells is based on their impedance response in conjunction with machine learning.

In impedance cytometry, we apply an AC voltage between a pair of electrodes, this results in current flowing through the system. A drop in ionic current or voltage across the electrodes occurs when the impedance of the particle crossing the pair of electrodes is relatively high compared to impedance of the buffer [29]. Electrical impedance cytometry thus allows screening of biological cells based on their dielectric properties. Figure 3.9 presents a simplified structure of an impedance cytometer. As microparticles (beads, biological cells etc.) pass through the electrodes, blockage of ionic currents results in voltage drop. The resulting peak information can then be extracted and used to analyze properties of biological particles.

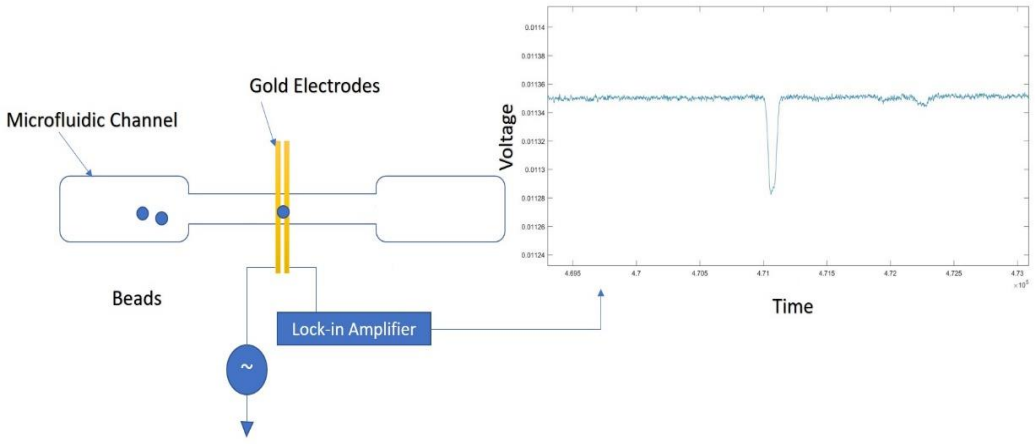

Figure 3.9. Simplified schematic of an impedance cytometer. Each peak corresponds to a single particle passing by.

In our system we conducted electrical measurements of cells across a wide range of frequencies. Multi-frequency impedance cytometry allows simultaneous probing of dielectric properties across a wide range of frequencies. In our design, we assumed an ideal polarizable electrode system with no faradic reactions as we used gold was the electrode material. When a voltage is applied across the two electrodes, it results in a double layer of ions with opposing polarity forming a boundary and acting as a capacitance, which is commonly referred to as the double-layer capacitance. A simplified circuit model proposed by Gawad et. al [30] to detect impedance change in the presence of cell along with the readout circuit is presented in figure 3.10. It consists of solution resistance (R_{sol}) parallel to membrane capacitance (C_m) and membrane resistance (R_m), which is in series with the double layer capacitance (C_{dl}).

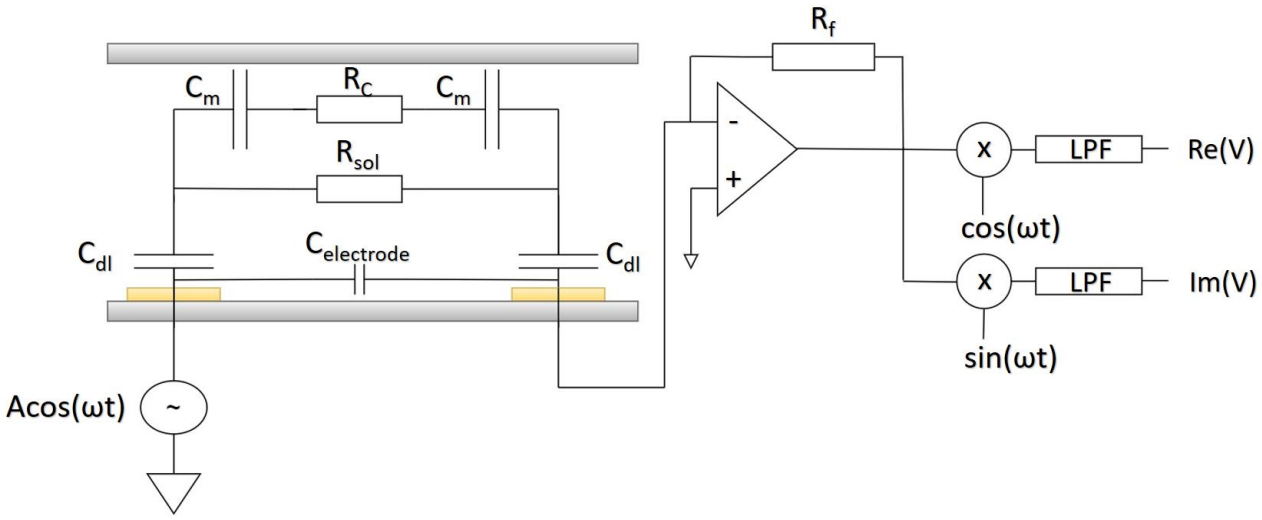

Fig 3.10 Equivalent circuit model of the electrode-electrolyte interface in the microchannel along with the readout circuit for measuring changes in resistance across the channel.

The change in impedance as each bead passes through the sensing region (Deblois and Bean 1970 [41]) is given as:

$$\Delta R = 2\rho_{sol}\frac{\left(\tan^{-1}\left(\frac{d}{2\sqrt{\frac{Ac}{\pi}-\frac{d^2}{4}}}\right)\right)}{\pi\sqrt{\frac{Ac}{\pi}-\frac{d^2}{4}}} - \frac{d}{2Ac} \qquad (1)$$

Where *Ac* is the area of the channel which is nothing but the product of height and length of the channel and ρ_{sol} is the resistivity of the solution. The change in amplitude of the signal when a cell passes through is:

$$\Delta I = \frac{\Delta R}{R^2}V_{in} \qquad (2)$$

3.5 Signal Processing and Machine Learning

The recorded data was then post processed using an algorithm to detrend and denoise the data which helped to analyze the cytometry data with minimal error. The algorithm was implemented in MATLAB®. Major part of this algorithm was developed and analyzed by Xinnan Cao from our group [31]. After detrending and denoising the data, peak location was found out using the *findpeaks* [32] function in MATLAB®. Based on the peak locations we implemented a code to find real and imaginary value of each peak. These values were further used to calculate electrical parameters of each peak.

Machine learning is a field of computer science that enables computers to learn without explicitly being programmed. Evolved from the study of pattern recognition and computational learning theory in artificial intelligence, machine learning plays a pivotal

role in the study and construction of algorithms which learn and make predictions on data. In machine learning, support vector machines (SVM's) are supervised learning models that have learning algorithms associated with it to analyze data for classification and regression [33]. SVM's are highly efficient in performing nonlinear classification, implicitly mapping their inputs to high dimensional feature spaces. Machine learning has found wide applications within biology and bioinformatics to make accurate predictions [34-36]. In the next chapter we discuss more about SVM to analyze cancer cell viability.

Chapter 4

Results and Discussions

We performed impedance cytometry measurements for the following viability percentages: 100% live cells, 100% dead cells, 50% live cells, 90% live cells and 82% live cells. Different viability percentages were obtained by exposing the drug to longer incubation periods. For 100% dead cells, we suspended live cancer cells in Phosphate Buffered Saline (PBS) for more than 72 hours. This resulted in lack of nutrition for cancer cells which ultimately led to 100% dead cells. Before performing the experiments, the viability was measured using trypan blue dye exclusion method. We conducted the measurements at 16 different frequencies ranging from 500KHz to 30 MHz.

Once the data was post processed and the real and imaginary value was found, we calculated amplitude change and phase change produced by each peak. Qualitatively, amplitude change is the change in impedance level when a cell pass by. It is the difference between the baseline voltage and the voltage when a cell passes by. Phase change is the change in angular position of the complex impedance when a cell passes by. We found the phase change and amplitude change for each single cell passing by and at all frequencies at which the measurements were conducted. In the following sections we discuss more about SVM classifier, performance of SVM classifier and discuss results obtained using our SVM classifier.

4.1 Support Vector Machine Classifier

Support Vector Machines (SVM's) are among the best "off-the-shelf" supervised learning algorithm widely used for classification and regression. In other words, provided a labeled training data which is nothing but supervised learning, the algorithm will output an optimal hyperplane which can categorize new examples (not used in the training data). To improve the classification accuracy, we used SVM with a Gaussian Kernel. A Kernel function is a form of mapping done to the training data to transform the data in higher dimensions. Using a kernel enables working with highly complex, efficient to compute data without using potentially infinite dimensional feature vectors. A Gaussian Kernel works on calculating the squared Euclidian distance between two feature vectors. The data used for training consisted of features extracted from 100% live and 100% dead cells. SVM algorithm with Gaussian Kernel was used in MATLAB®.

For training the data we labeled the features from live cells as 1 and features from live cells as 0. Features were nothing but individual properties of measured phenomenon. Our feature matrix contained a matrix of amplitude change and phase change at different frequencies. Rows corresponded to features and columns corresponded to training data points (amplitude and phase change of each peak at different frequencies). Training data size was more than 1000 samples to make sure the SVM classifier does not face problem of over fitting. As the number of features were reasonable, we did not face the problem of underfitting. To test the robustness and accuracy of our SVM classifier, we tested it three different viability percentages (90% live, 50% live and 82% live). The number of 1's predicted by the SVM classifier divided by the total number of samples/data points gave us the viability percentage predicted by the SVM classifier.

4.2 Performance of the SVM Classifier

To evaluate the performance of our SVM classifier, we used confusion matrix on a set of test data for which the true values were known. A part of training data which included features from 100% live and 100% dead cells was used for testing which then built the confusion matrix. Following performance metrics which helped us evaluate the SVM classifier:

$$Accuracy = (T.P. + T.N.)/N \quad (3)$$

Where True Positives (T.P.) is the number of times the classifier predicts the cell was live, given that the cell was live, True Negatives (T.N.) is the number of times the classifier predicts the cell was dead, given that the cell was dead and N is the number of data points used for training.

Similarly, False Positives (F.P.) is the number of times the classifier predicts the cell is live, given the cell was dead and False Negatives (F.N.) is the number of the times the classifier predicts the cell was dead, given the cell was live.

Based on this performance metrics we build a confusion matrix which helped us to analyze the results in detail. Generally false positives in our case are undesirable. Predicting a live cancer cell to be dead can lead to severe loss of life.

4.3 Amplitude Change as a feature for classification

We explored the amplitude change at different frequencies as features for our SVM classifier. Figure 4.1 and 4.2 represents normalized impedance response of live cancer cells and dead cancer cells at 500KHz,20MHz and 30MHz. Higher frequencies (> 10MHz) probe the internal properties of the cell [22].

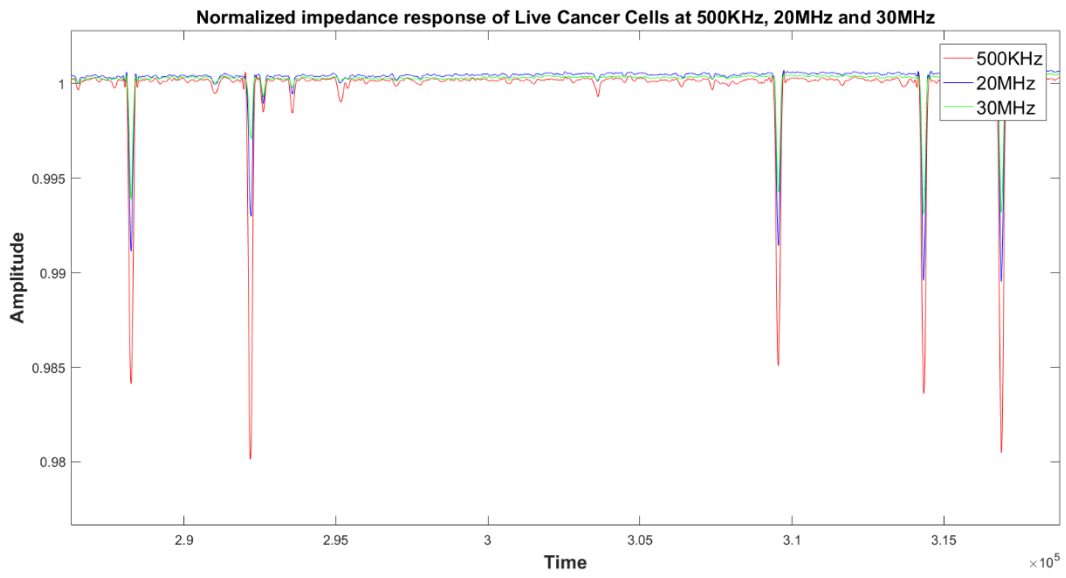

Figure 4.1. Normalized impedance response of live cancer cells at 500KHz, 20MHz and 30MHz. Each peak corresponds to a single cell passing by.

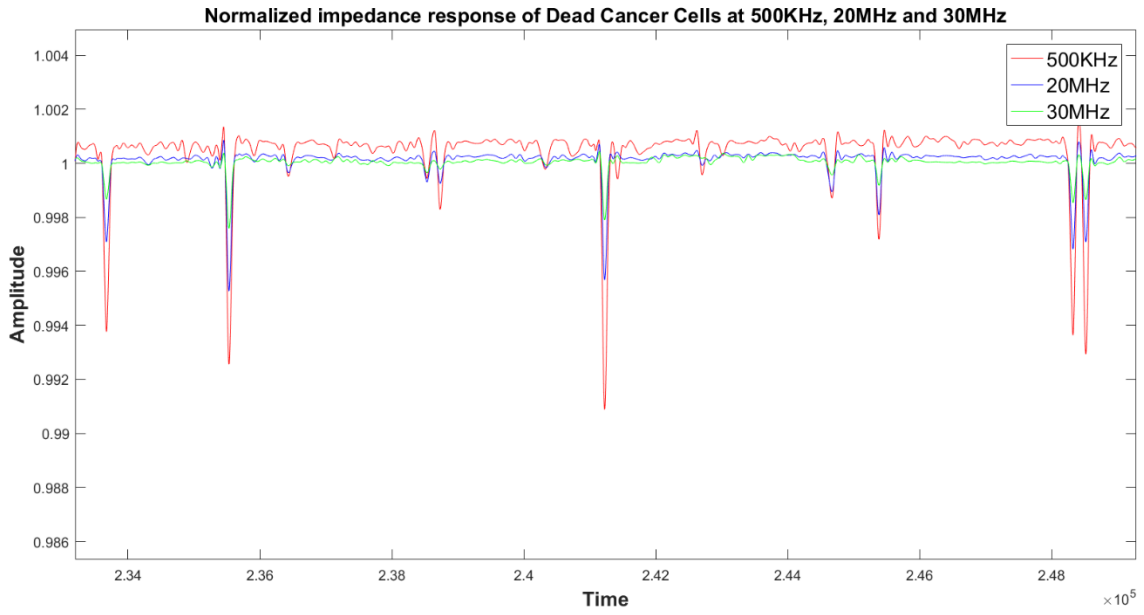

Figure 4.2 Normalized impedance response of dead cancer cells at 500KHz, 20MHz and 30MHz. Each peak corresponds to a single cell passing by.

At higher frequencies we not only probe the internal properties of the cell but also distinguish live and dead cells based on size. As a cell dies, it's size tend to shrink. Figure 4.3 presents the amplitude spectrum of live cancer cells and dead cancer cells across a wide range of frequencies. Also, from the scatter plot at different frequencies we can visually distinguish between live and dead cancer cells. Figure 4.4, 4.5 and 4.6 presents scatter plot of live cancer cells and dead cancer at different frequencies.

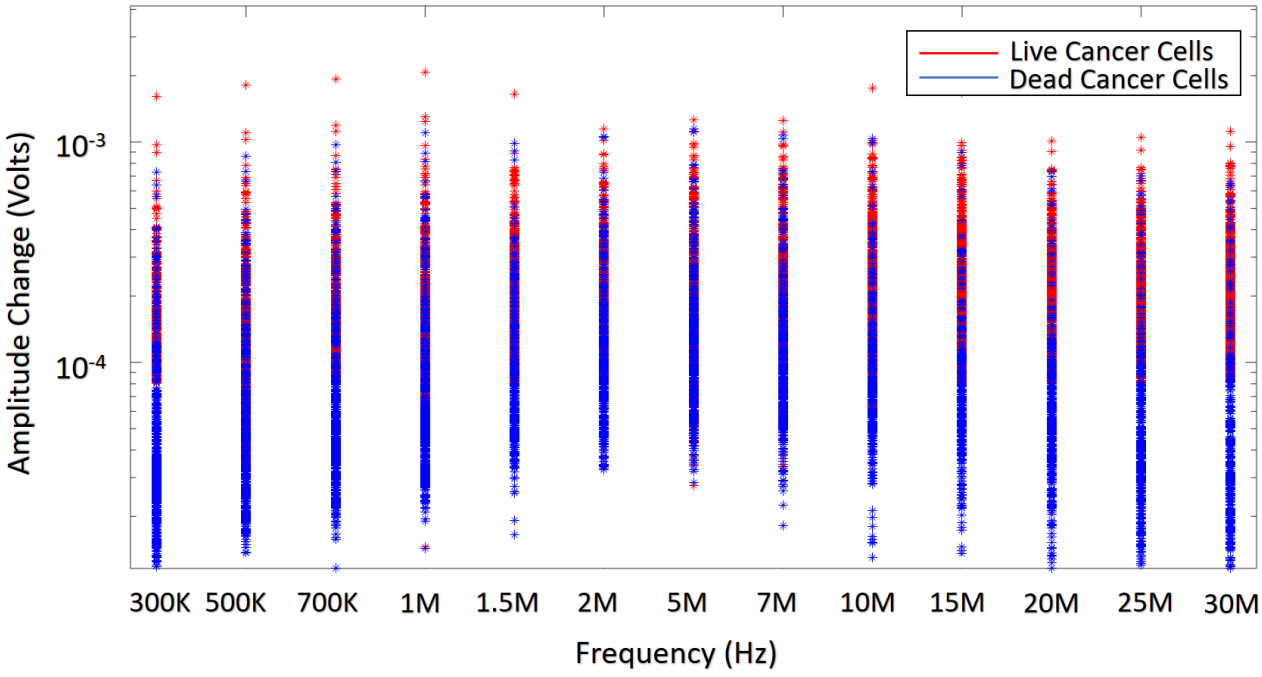

Figure 4.3. Amplitude spectrum of live cancer cells and dead cancer cells from 500KHz to 30MHz frequency.

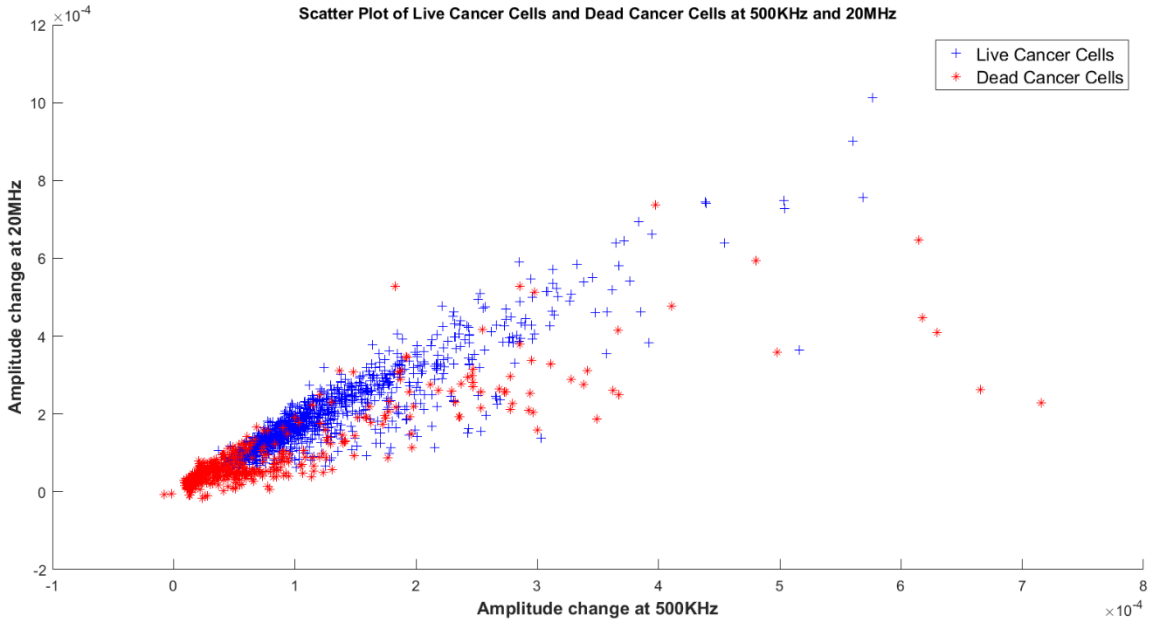

Figure 4.4. Scatter plot of live cancer cells and dead cancer cells at 500KHz and 20MHz.

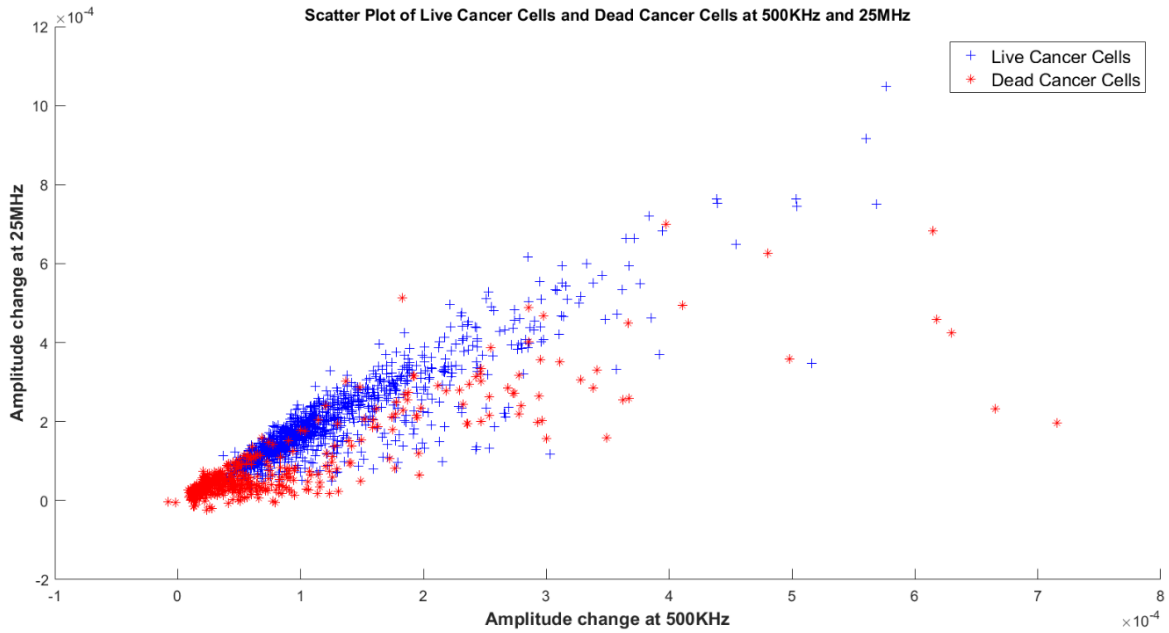

Figure 4.5. Scatter plot of live cancer cells and dead cancer cells at 500KHz and 25 MHz.

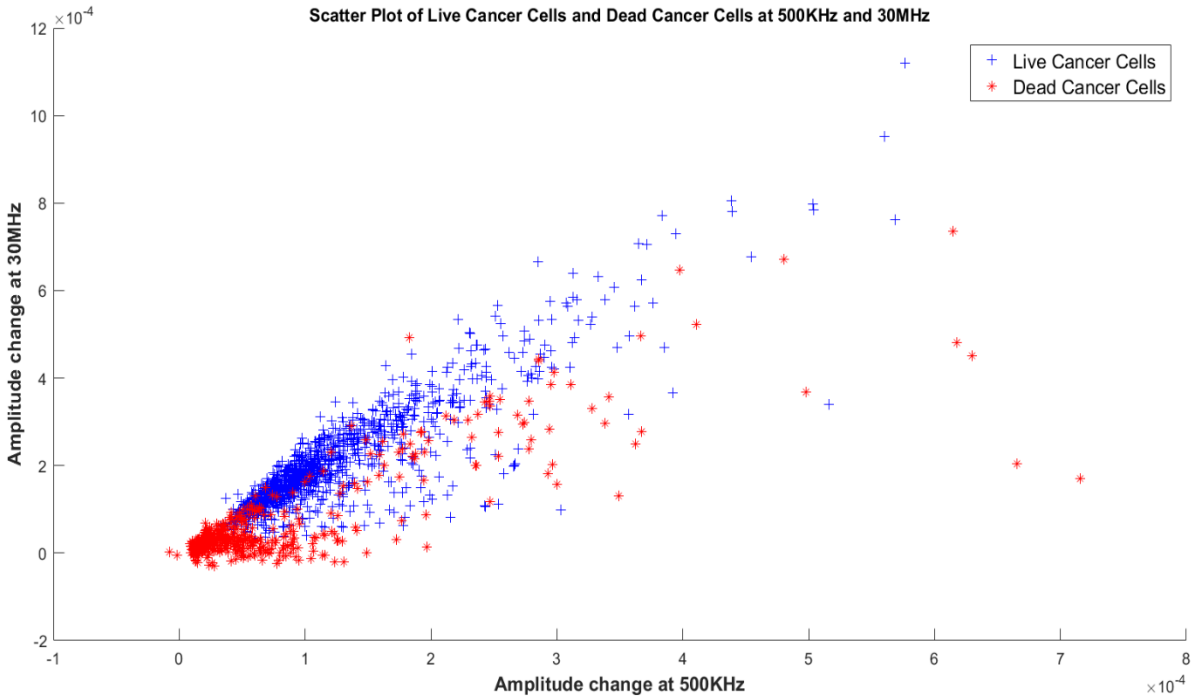

Figure 4.6. Scatter plot of live cancer cells and dead cancer cells at 500KHz and 30MHz.

We used the amplitude change at 4 different frequencies (500kHz, 20MHz, 25MHz and 30MHz) to train our SVM classifier with gaussian kernel. We then tested the SVM model with the amplitude change data from different viability percentages of cancer cells. The confusion matrix for the SVM classifier using amplitude change as feature is shown in figure 4.7. Our classifier reported to have an accuracy of **89.7%**, True Positive Rate and True Negative Rate of **90%** each. Figure 4.8 represents a bar graph comparing between the analysis of cell viability by trypan blue dye exclusion method (ground truth) and multi-frequency impedance spectroscopy with SVM using amplitude change as features for the SVM classifier.

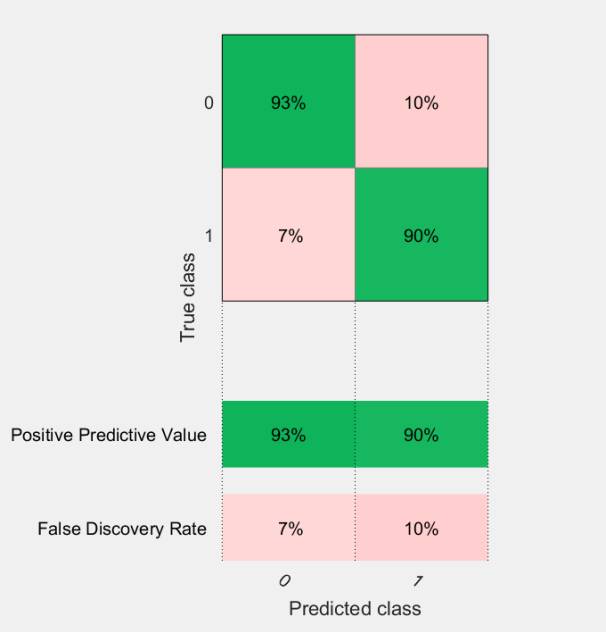

Figure 4.7. Confusion matrix of the SVM classifier while using impedance change as features while training the SVM.

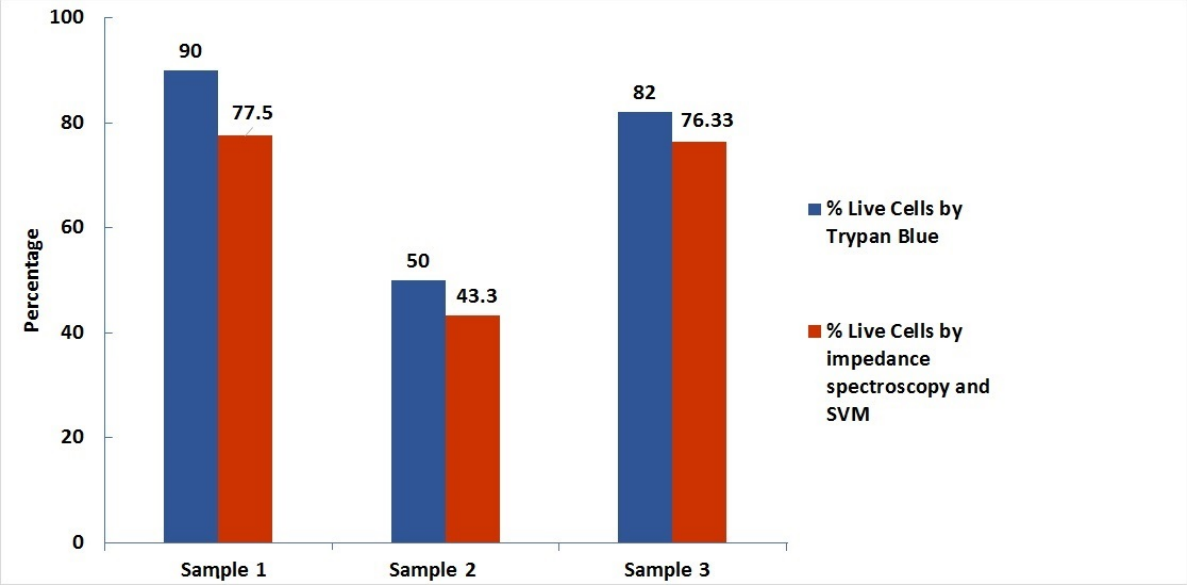

Figure 4.8. Comparison between the analysis of cell viability by trypan blue staining method (ground truth) and multi-frequency impedance spectroscopy with SVM using impedance change as features for the SVM classifier.

4.4 Phase Change as Feature for Classification

As discussed previously, whenever a cell passes by, it results in a momentary change in the position of complex impedance. We defined phase change as the difference of inverse tangent of imaginary to real part when a cell passes through the electrodes. For phase change, we observed a general trend wherein phase change was negative at lower frequencies (<1MHz) and positive at higher frequencies. Figure 4.9, 4.10 and 4.11 presents scatter plots representing phase change for live cancer cells and dead cancer cells at various frequencies. We tested our SVM classifier for all the 4 frequency sets. The frequency set consisting of phase change at 500KHz, 20MHz, 25MHz and 30MHz reported to have higher accuracy and accurate predictions for different viability percentages.

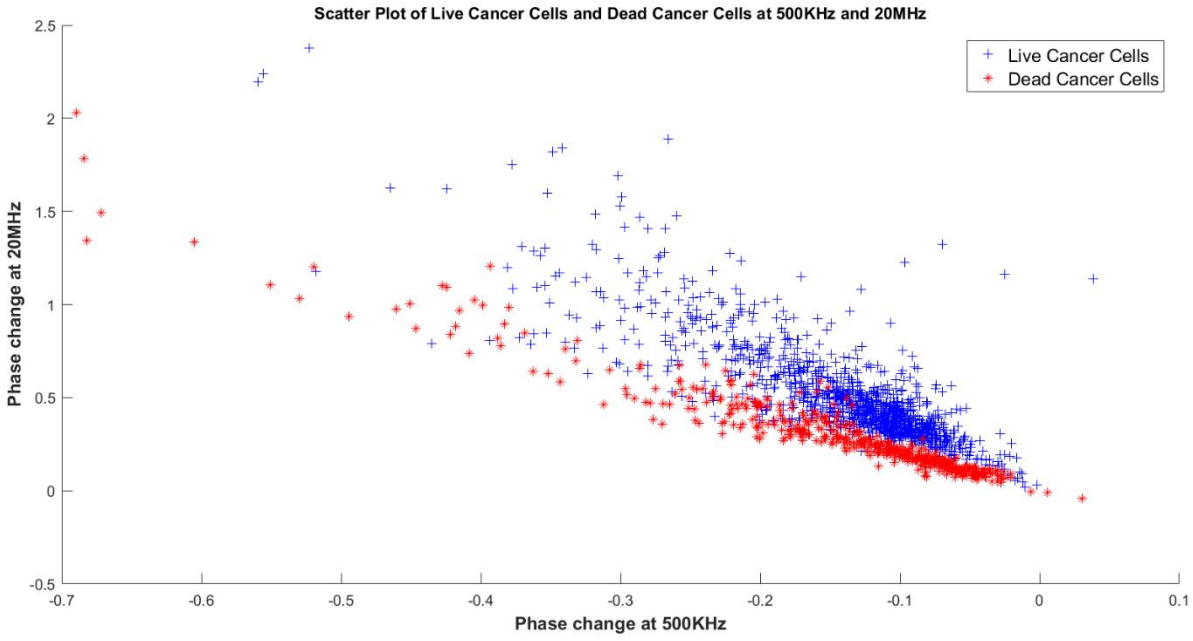

Figure 4.9. Scatter plot of live cancer cells and dead cancer cells representing phase change at 500KHz and 20MHz.

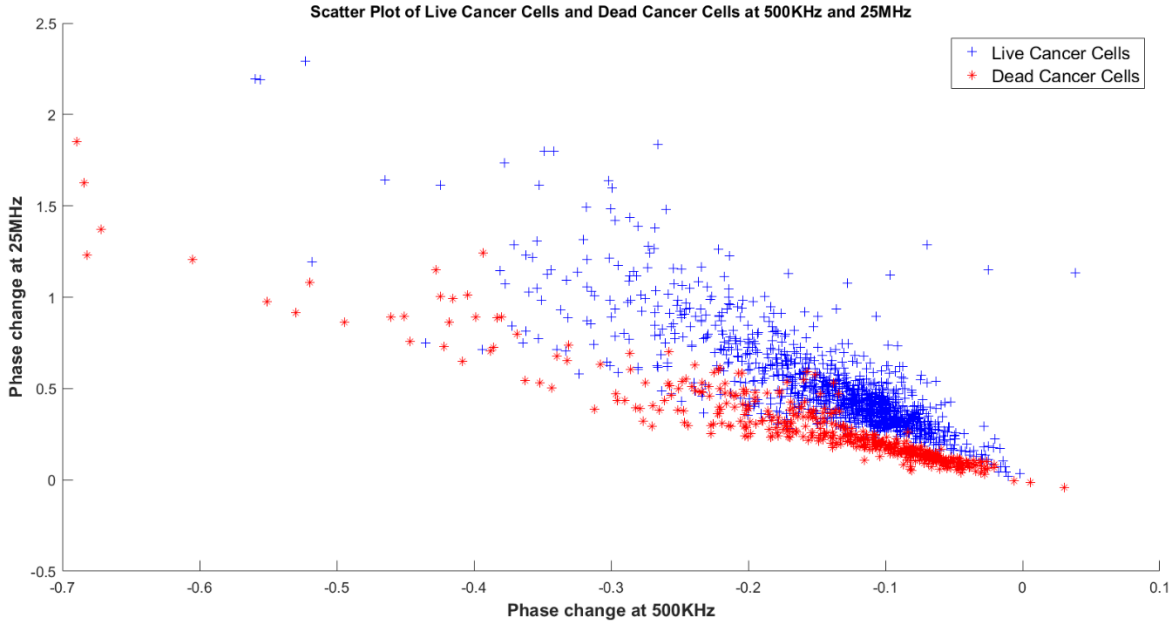

Figure 4.10. Scatter plots of live cancer cells and dead cancer cells representing phase change at 500KHz and 25MHz.

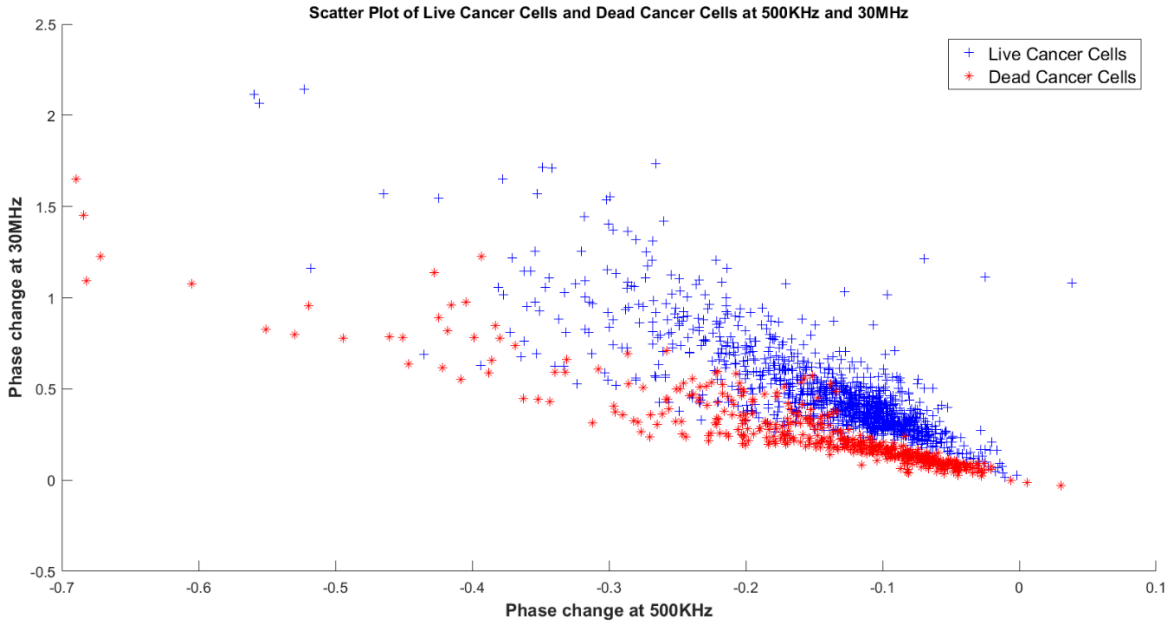

Figure 4.11. Scatter plots of live cancer cells and dead cancer cells representing phase change at 500KHz and 30MHz.

The confusion matrix for the SVM classifier using phase change as feature is shown in figure 4.12. Our classifier reported to have an accuracy of **90.6%**, True Positive Rate of **90%** and True Negative Rate of **93%**. Figure 4.13 represents a bar graph comparing between the analysis of cell viability by trypan blue dye exclusion method (ground truth) and multi-frequency impedance spectroscopy with SVM using phase change as features for the SVM classifier.

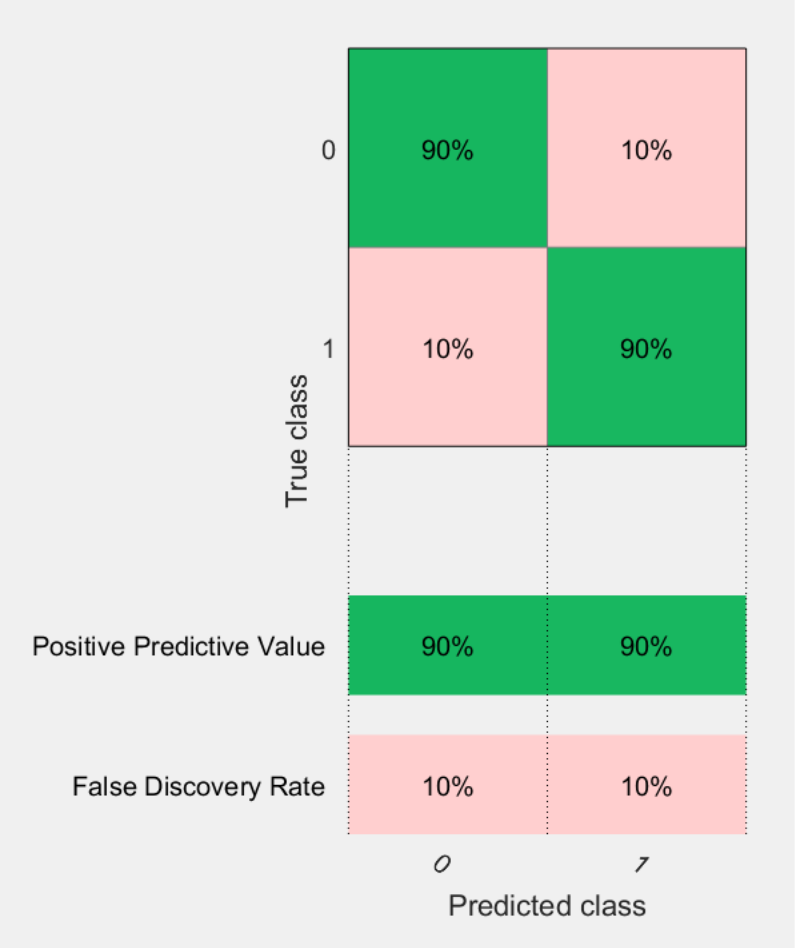

Figure 4.12. Confusion matrix of the SVM classifier while using phase change as features while training the SVM.

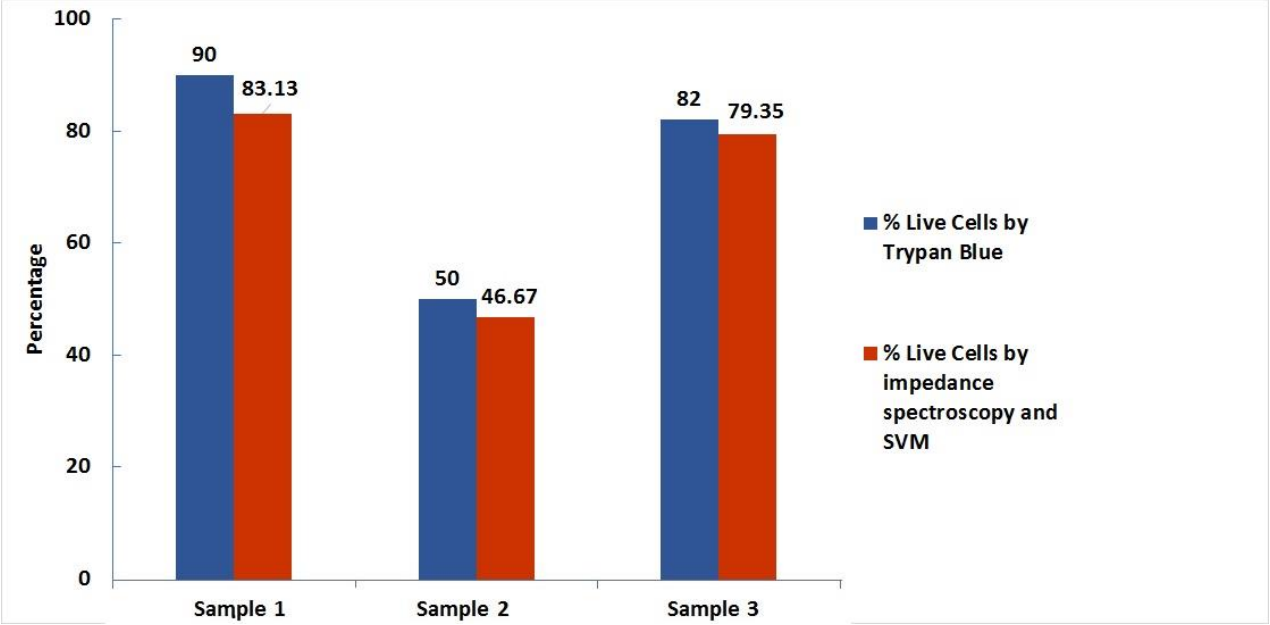

Figure 4.13. Comparison between the analysis of cell viability by trypan blue staining method (ground truth) and multi-frequency impedance spectroscopy with SVM using phase change as features for the SVM classifier.

4.5 Amplitude Change and Phase Change as features for the SVM classifier

Lastly, we explored using amplitude change and phase change as features for the SVM classifier. Since for the same frequency sets (500KHz, 20 MHz, 25 MHz and 30 MHz) amplitude change and phase change individually gave good results we built an 8-feature matrix which included both amplitude change and phase change. Before training the 8-feature matrix with the SVM classifier the data points were normalized to ensure that all the data points lie within a specified range. Normalizing the data helps any machine learning classifier to perform faster. The confusion matrix for the SVM classifier amplitude change and phase change as features is shown in figure 4.14. Our classifier reported to

have an accuracy of **95.9%**, True positive Rate of **95%** and True Negative Rate of **97%**. Figure 4.15 represents a bar graph comparing between the analysis of cell viability by trypan blue dye exclusion method (ground truth) and multi-frequency impedance spectroscopy with SVM using phase change as features for the SVM classifier. In all the three different scenarios the trained SVM model could predict viability accurately. While phase change followed a general trend (negative at lower frequencies and positive at higher frequencies), the actual value of phase change helped to classify between live and dead cells.

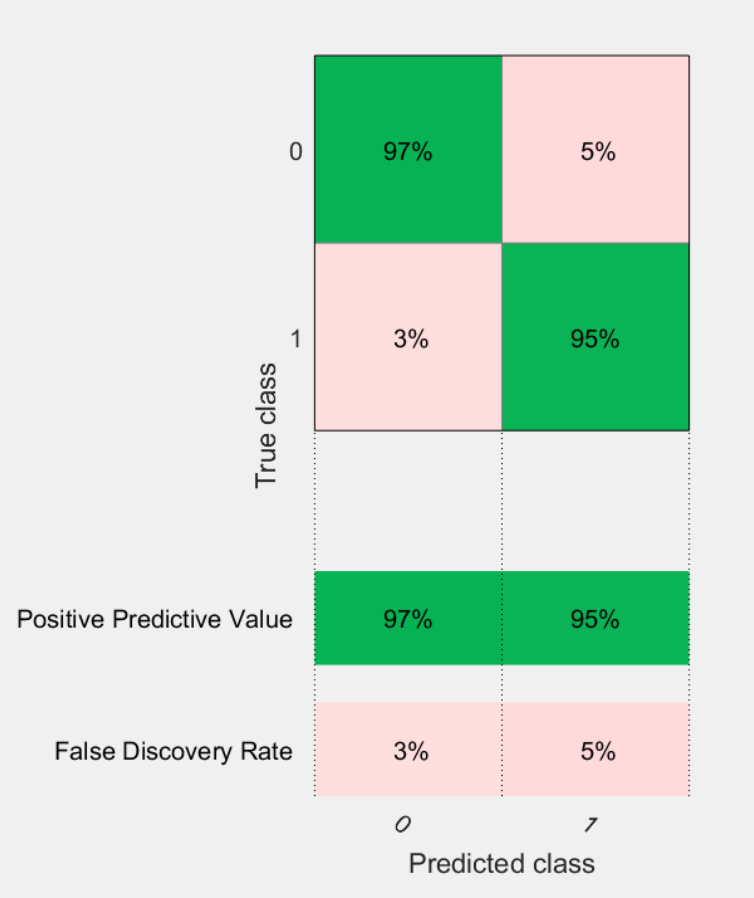

Figure 4.14. Confusion matrix of the SVM classifier while using phase change and amplitude change as features while training the SVM.

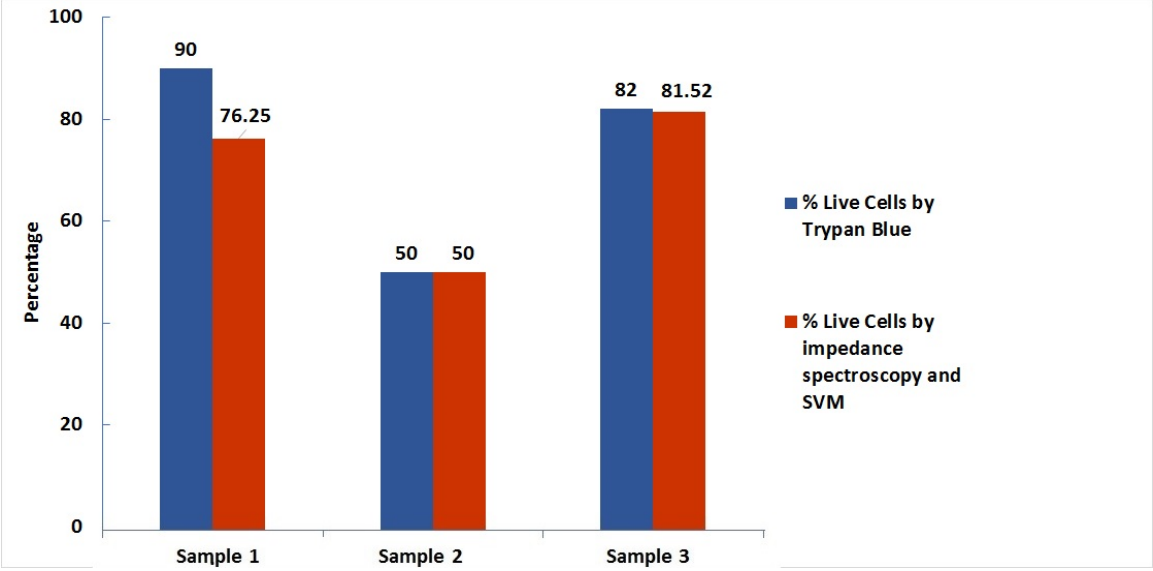

Figure 4.15. Comparison between the analysis of cell viability by trypan blue staining method (ground truth) and multi-frequency impedance spectroscopy with SVM using phase change and impedance change as features for the SVM classifier.

Chapter 5

Exploring Use of Impedance Cytometry for Quantification of Cancer Cells in Blood Cells

We extended our work to explore use of impedance cytometry to quantify cancer cells in blood cells. In the past many methods have been proposed for cancer cell detection, characterization and separation including chromatography, magnetic activated cell sorting and di-electrophoresis [38,39]. Currently commercially available devices to isolate and characterize cancer cells from blood rely on size based separation or by using surface antigens like epithelial cell adhesion molecule (EpCAM). Here we demonstrate a novel method to rapidly characterize cancer cells from blood by referring to phase change in impedance cytometry. This helps to electrically classify cancer cells from whole blood, rather than relying on size only.

Figure 5.1 shows the schematic diagram of our experimental setup. This includes a microfluidic channel embedded on glass wafer with gold electrodes, a multi-frequency lock in amplifier (Zurich Instruments ®), and software to record to analyze the data. The schematic is like the one used in previous experiments, where we relied on phase change only to quantify cancer cells from blood.

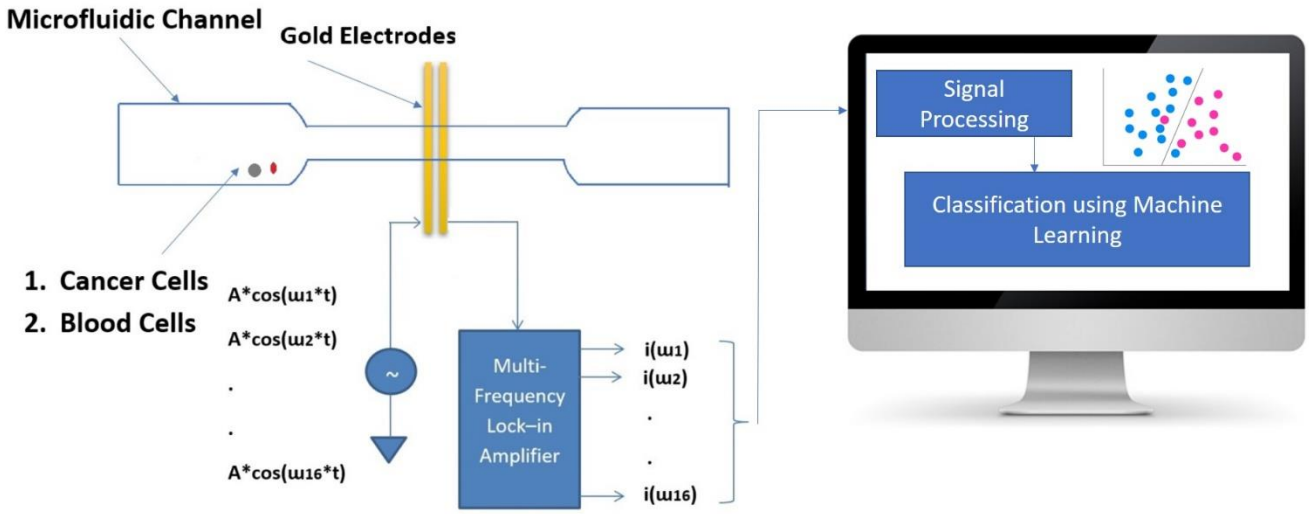

Figure 5.1. Schematic Diagram of the system. Multi-frequency impedance cytometry measures the response over a broad range of frequencies.

We measured the impedance response of breast cancer cells (t47d) and healthy blood. These cells were suspended in Phosphate Buffered Saline. The impedance response of cancer cells and blood cells was recorded at 16 different frequencies ranging from 500KHz to 30MHz. The recorded data was then processed and analyzed in MATLAB. We implemented different machine learning classifiers for accurate classification. The classifiers used were namely Logistic Regression, K Nearest Neighbors and Support Vector Machine.

Passage of beads/cells over the sensor electrodes in the microfluidic channel results in modulation of impedance. This momentarily changes the angular position (phase) of the complex impedance when a cell passes by. Figure 5.2 and 5.3 represent scatter plots of phase change for blood and cancer cells at different frequencies and figure 5.4 represents

normalized impedance response for cancer cells at different frequencies. Normalized impedance response for blood cells in represented in Figure 5.5.

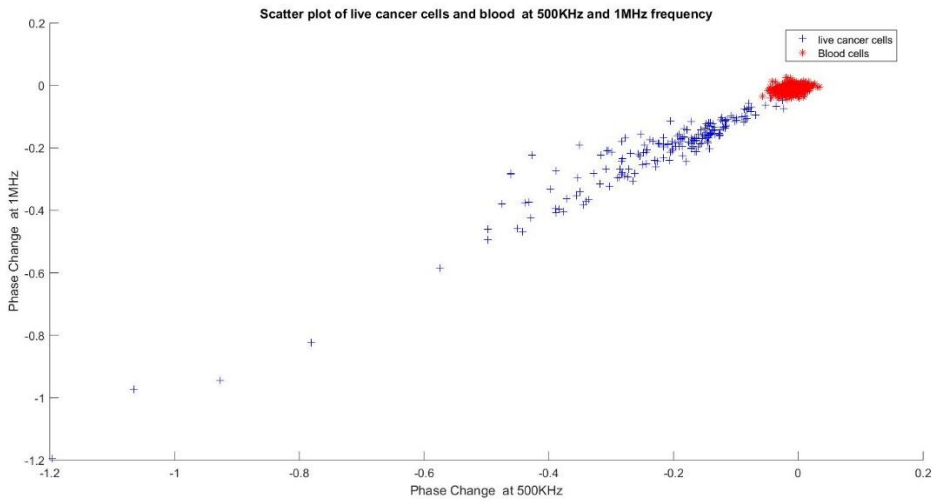

Figure 5.2. Scatter plots of phase change for live cancer cells and whole blood cells at 500KHz and 1MHz.

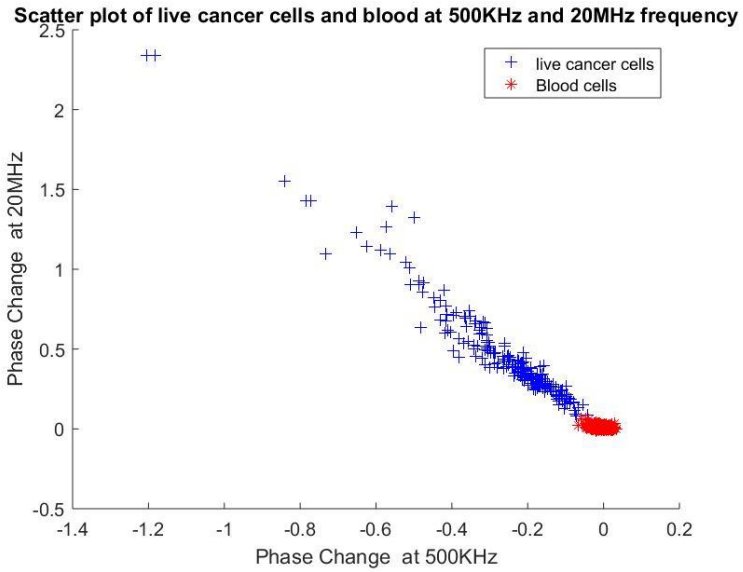

Figure 5.3. Scatter plots of phase change for live cancer cells and whole blood cells at 500KHz and 20MHz.

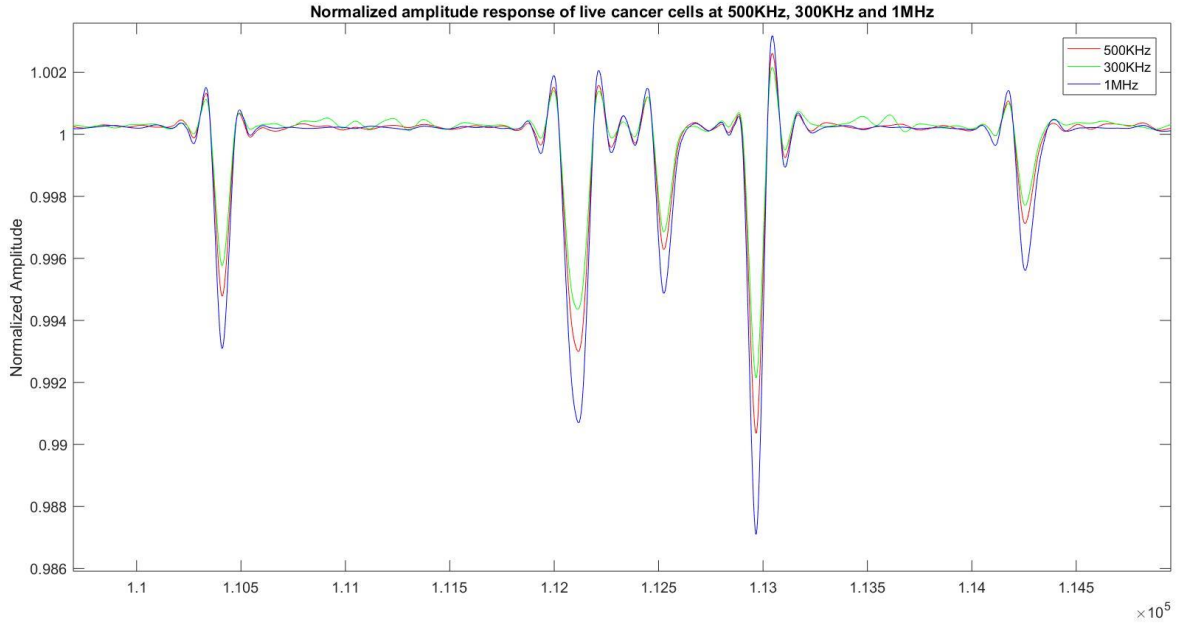

Figure 5.4. Normalized amplitude response of live cancer cells at 500KKz, 300KHz and 1MHz.

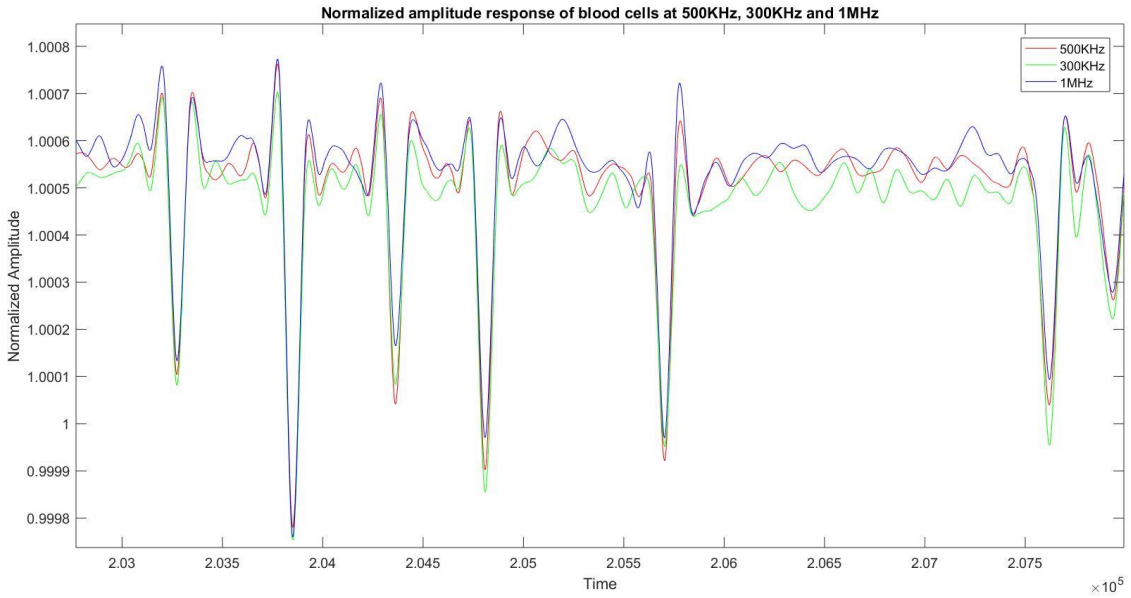

Figure 5.5. Normalized amplitude response of whole blood cells at 500KKz, 300KHz and 1MHz.

From the scatter plot, we see that visual inspection helps us clearly differentiate between cancer cells and blood cells, machine learning algorithms are implemented to enable higher classification accuracy in a higher dimension. Table 5.1 represents accuracy in percentage of different machine learning classifiers like Logistic Regression, K Nearest Neighbors and Support Vector Machine. We are successfully able to distinguish between cultured cancer cells and whole blood using phase properties of a cell obtained from impedance cytometry data.

Classifier	Accuracy to classify between blood cells and cancer cells.
Logistic Regression	**99.5%**
K Nearest Neighbors	**99.2%**
Support Vector Machine	**98.6%**

Table 5.1. Accuracy of different machine learning classifiers to classify between blood cells and cancer cells.

Chapter 6

Conclusion and Future Scope

In this work we present a novel method to rapidly assess patient response to targeted cancer therapy using multi-frequency impedance cytometry and supervised machine learning. Our SVM classifier reported to have high accuracy which rightly matched with the ground truth i.e. trypan blue dye exclusion method. We were also able to effectively analyze impedance cytometry data and use electrical properties, like amplitude change and phase change to analyze viability of cancer cells. We found that phase change follows a trend wherein phase change is negative at lower frequencies and positive at higher frequencies, but the quantitative change in phase for different type of cells helps accurate classification. Compared to optical techniques for label free analysis of cell viability our novel method can rapidly analyze cell viability with minimal cost.

We also explored use of impedance cytometry to quantify cancer cells from blood cells. The heterogeneity between cancer cells and blood allows us to rapidly measure their properties. We envision this preliminary result as benchmark which can further be used to accurately quantify circulating tumor cells from blood in patients. This quantification helps to characterize cancer cells using their electrical properties rather than size which can yield more accurate results. We envision using this device as a point-of-care diagnostic for assessing patient response and personalization of therapeutics.

Chapter 7

Appendix

7.1 Oxygen Plasma Etching

PDMS is usually hydrophobic in nature. Surface treatment is believed to expose silanol (OH) groups at the surface of PDMS that when brought together form Si---O---Si covalent bonds. Oxygen plasma thus changes the surface properties of PDMS to render it hydrophilic [37].

7.2 Support Vector Machine

In this section we discuss more about support vector machine and the mathematics behind it. Given a set of points x_i in an n dimensional space with the corresponding classes $\{y_i : y_i \in \{-1,1\}\}$then the SVM training algorithm will attempt to place a hyperplane between the points {-1,1}. A new pattern x can then be classified by testing which side of the hyper plane the point lies on.

For classification, given a training data, suppose the two classes can be separated by a hyperplane

$$(\omega x) + b = 0 \quad (1)$$

Let us assume that all the training data satisfies the following constraints to describe the separating hyperplane:

$$(\omega . x_i) + b \geq +1 \; for \; y_i = +1 \quad (2)$$

$$(\omega . x_i) + b \leq -1 \; for \; y_i = -1 \quad (3)$$

This can be then combined into one set of inequalities. These equations can be solved to find which points lie on the two planes. The optimal solution can be found by solving the equation:

$$argmax \sum_{k} \alpha_j - 0.5 \sum_{j,k} \alpha_j \alpha_k y_j y_k (x_j x_k) \tag{4}$$

Once we have found the vector α the margin can be computed with the equation:

$$\omega = \sum_{j} \alpha_j x_j \tag{5}$$

Upon analysis of the equation, we find that the solution has a single global optimum which can be found efficiently.

Bibliography

[1]. Stewart, B. W. & Wild, C. International Agency for Research on Cancer & World Health Organization. *World cancer report 2014*. (International Agency for Research on Cancer WHO Press, 2014).

[2]. National Cancer Institute, (February 9, 2015), *What is Cancer?* Retrieved from https://www.cancer.gov/about-cancer/understanding/what-is-cancer.

[3]. Wagman LD. "Principles of Surgical Oncology" in Pazdur R, Wagman LD, Camphausen KA, Hoskins WJ (Eds*) Cancer Management: A Multidisciplinary Approach*. 11th edition. 2008.

[4]. Rachel Airley (2009). *Cancer chemotherapy*. Wiley-Blackwell. ISBN 0-470-09254-8.

[5]. CK Bomford, IH Kunkler, J Walter. Walter and Miller's Textbook of Radiation therapy (6th Ed), page 311.

[6]. Laurence L. Brunton, editor-in-chief; John S. Lazo and Keith L. Parker, Associate Editors (2006). *Goodman & Gilman's The Pharmacological Basis of Therapeutics* (11th ed.). United States of America: The McGraw-Hill Companies, Inc. ISBN 0-07-142280-3.

[7]. National Cancer Institute, *NCI Dictionary of Cancer Terms*, Retrieved from https://www.cancer.gov/publications/dictionaries/cancer-terms/def/targeted-therapy.

[8]. National Cancer Institute, *NCI Dictionary of Cancer Terms,* Retrieved July 15, 2014.

[9]. Sawyers, C. (2004). Targeted cancer therapy. *Nature*, 432(7015), 294-7.

[10]. American Society of Clinical Oncology, *Understanding Targeted Cancer Therapy*, Retrieved March 10, 2018.

[11]. C. Jin, S. M. McFaul S. P. Duffy, X. Deng, P. Tavassoli, P. C. Black and H. Ma, "Technologies for label-free separation of circulating tumor cells: from historical foundations to recent developments," *Lab on a Chip*, **14(1)**, 32-44, 2014.

[12]. O.D. Laerum, T. Farsund, Clinical application of flow cytometry: a review, cytometry 2(1) (1981) 1-13.

[13]. Mok Janine, Michael N. Mindrinos, Ronald W. Davis, Mehdi Javanmard, Digital microfluidic assay for protein detection, Proceedings of National Academy of Sciences 111(6) (2014) 2110-2115.

[14]. M. Javanmard, R. W. Davis, A microfluidic platform for electrical detection of DNA hybridization, Sens.Actuators B: Chem 154(1) (2011) 22-27.

[15]. W. Strober, *Monitoring Cell Growth* Wiley Online Library, DOI: 10.1002/0471142735.ima03as2.

[16]. Wikipedia, *Optical Coherence Tomography*, Retrieved March 10, 2018.

[17]. Huang, D. et al. Optical coherence tomography. Science 254, 1178–1181 (1991).

[18]. Y. Jung, O. J. Klein, H. Wang and C. Evans, "Longitudinal, label-free, quantitative tracking of cell death and viability in a 3D tumor model with OCT", Nature Scientific Reports, 2016

[19]. Ho¨ber R (1910) Eine Methode die elektrische Leitfaehigkeit im Innern von Zellenzu messen. Arch Ges Physiol 133:237–259.

[20]. Ho¨ber R (1912) Ein zweites Verfahren die Leitfaehigkeit im Innern von Zellen ze messem. Arch Ges Physiol 148:189–221.

[21]. Ho¨ber R (1913) Messungen der inne.

[22]. Sun T., Mogran H. Single-cell microfluidic impedance cytometry: a review, Microfluid Nanofluid (2010) 8:423–44.

[23]. Holmes D., Pettigrew D., Reccius C H., Gwyer J. D., Berkel C., Holloway J., Davies D. E. and Morgan H, Leukocyte analysis and differentiation using high speed microfluidic single cell impedance cytometry, *Lab on a Chip*, 2009, **9**, 2881-2889.

[24]. Evander M., Ricco A. J., Morser J., Kovacs G. T. A., Leung L. L. K. and Giovangrandi. Microfluidic impedance cytometer for platelet analysis. *Lab on a Chip*, 2013,**13**, 722-729, doi: 10.1039/C2LC40896A.

[25]. Simon P., Frakowski M., Bock N. and Neukammer J., Label-free whole blood cell differentiation based on multiple frequency AC impedance and light scattering analysis in a micro flow cytometer. *Lab on a Chip*, 2016, **16**, 2326.

[26]. Xie P., Cao X., Lin Z. and Javanmard M., Top-down fabrication meets bottom-up synthesis for nanoelectronic barcoding of microparticles. *Lab on a Chip*, 2017,**17**, 1939-1947.

[27]. Zhao, Y. *et al.* Tumor cell characterization and classification based on cellular specific membrane capacitance and cytoplasm conductivity. *Biosensors and Bioelectronics*, **57,** 245–253 (2014).

[28]. Z. Lin, X. Cao, P. Xie, M. Liu and Mehdi Javanmard, PicoMolar level detection of protein biomarkers based on electronic sizing of bead aggregates: theoretical and experimental considerations. *Biomed Microdevices*. vol. 17, no. 6, pp. 119, 2015.

[29]. S. Emaminjed, M. Javanmard, R.W. Duton, R.W. Davis, Microfluidic diagnostic tool for the developing world: contactless impedance flow cytometry, *Lab on a Chip*, **12**(no. 21) (2012) 4499

[30]. S. Gawad, L. Schild and Ph. Renaud, Micromachined impedance spectroscopy flow cytometer for cell analysis and particle sizing, *Lab on a Chip*, 2001, **1**,76-82.

[31]. Cao X., Detrending and denoising of impedance cytometry data, Retrieved Rutgers University online libraries.

[32]. Find peaks function, *MATLAB,* Retrieved March 10, 2018.

[33]. Cotres, C. & Vapnik, V. Machine Learning (1995) 20:273. https://doi.org/10.1007/BF00994018.

[34]. Wong, S.L. et al. Combining biological networks to predict genetic interactions. *Proceedings of National Academy of Science*. USA **101**, 15682–15687.

[35]. Middendorf, M., Kundaje, A., Wiggins, C., Freund, Y. & Leslie, C. Predicting genetic regulatory response using classification. Bioinformatics 20, i232–i240.

[36]. Allen, J.E., Majoros, W.H., Pertea, M. & Salzberg, S.L. JIGSAW, GeneZilla, and GlimmerHMM: puzzling out the features of human genes in the ENCODE regions. Genome Biol. 7 Suppl, S9 (2006).

[37]. S. H. Tan, N. Nguyen, and C. Chua, "Oxygen plasma treatment for reducing hydrophobicity of a sealed polydimethylsiloxane microchannel," pp. 1–9, 2010.

[38]. Komen J., Wolbes F., Franke H. R., Andersson H., Vermes I., Berg A., Viability analysis and apoptosis induction of breast cancer cells in a microfluidic device: effect of cytostatic drugs, *Biomed Microdevices*. 2008, 7:727

[39]. Swasthika S., Vanapali S., Microfluidic cell isolation technology for drug testing of single tumor cells and their clusters, *Nature Scientific Reports*, **7**, Article number: 41707.

[40]. Mazutis L., Gilbert J., Ung W.L., Weitz D., Griffiths A., Heyman J. A., Single-cell analysis and sorting using droplet-based microfluidics, Nature Protocols volume **8**, pages 870–891 (2013).

[41]. R. W. DeBlois, C. P. Bean, Rev. of Sci. Inst. 41(7), 909–916 (1970)